Title	Instrumented concrete pile tests – part 2: strain interpretation
Author(s)	Flynn, Kevin N.; McCabe, Bryan A.
Publication Date	2021-11-03
Publication Information	Flynn, Kevin N., & McCabe, Bryan A. (2022). Instrumented concrete pile tests – part 2: strain interpretation. Proceedings of the Institution of Civil Engineers - Geotechnical Engineering, 175(1), 112-135. doi:10.1680/jgeen.21.00127
Publisher	ICE Publishing
Link to publisher's version	https://doi.org/10.1680/jgeen.21.00127
Item record	http://hdl.handle.net/10379/17133
DOI	http://dx.doi.org/10.1680/jgeen.21.00127

Instrumented Concrete Pile Tests – Part 2: Strain Interpretation

Kevin N. Flynn BA BAI PhD CEng MIEI, Principal Geotechnical Engineer, AGL Consulting Geotechnical Engineers, Sandyford, Dublin 18, Ireland.

Bryan A. McCabe BA BAI PhD CEng FIEI, Senior Lecturer, School of Engineering, National University of Ireland, Galway, Ireland.

E-mail: bryan.mccabe@nuigalway.ie

ABSTRACT:

The incorporation of strain gauges (traditionally electrical resistance and vibrating wire gauges but increasingly fibre optic sensors) within concrete piles provides a valuable opportunity for enhanced understanding of shear stress distribution along the pile shaft and bearing resistance at the pile base. This paper provides a much-needed roadmap for practitioners to negotiate the challenges associated with strain interpretation in concrete piles. Key learnings from the paper relate to residual loads, temperature effects during curing, pile bending, strain-dependent modulus, unload-reload loops and creep strains during loading. Guidance is drawn from a combination of techniques advocated in the literature, examples from the authors' experiences from various instrumented concrete pile types, as well as case histories published by others.

KEYWORDS: cast in situ, concrete, piles, instrumentation, load test, strain gauge

INTRODUCTION

The advent of cost-effective, commercially-available instrumentation offers possibilities for more judicious use of load tests on concrete piles. However, interpretation of strain measurements from the instrumentation can be challenging, often hampered by pile installation and curing effects, bending and concrete modulus issues, load testing procedures and malfunctioned gauges. Unfortunately, the literature on strain interpretation in concrete piles is relatively sparse and, in certain instances, contradictory, and there is no single resource that practitioners can resort to for guidance. Drawing on some literature for data interpretation, in addition to specific examples from the authors' experiences of various instrumented cast-in-situ types and some published by others, this paper aims to bring clarity to the strain interpretation process through a step-by-step guide. This paper is best studied in conjunction with the companion paper (Flynn and McCabe 2021b) covering a review of instrumentation types and procedures. The intention of the paper is to equip the practitioner with an understanding that will ultimately espouse the more widespread use of instrumented piles.

BACKGROUND AND DATABASE

The magnitude of load (P) at a specific level within an instrumented concrete pile is given by:

$$P = E_{pile}A_{pile}\varepsilon_{elastic} \tag{1}$$

where E_{pile} is the pile's elastic modulus, A_{pile} is the pile cross-sectional area and $\varepsilon_{elastic}$ is the mobilised elastic strain. Flynn and McCabe (2021b) discuss suitable instrumentation for accurate measurement (and inference of axial load using Equation 1); these measure total strain ε_{total}, comprising the following components:

$$\varepsilon_{total} = \varepsilon_{mech} + \varepsilon_{thermal} = \varepsilon_{elastic} + \varepsilon_{creep} + \varepsilon_{thermal} \tag{2}$$

where ε_{mech} is mechanical strain within the pile, which comprises the elastic strain $\varepsilon_{elastic}$ and (irreversible) creep strain ε_{creep}, and $\varepsilon_{thermal}$ is strain induced by temperature changes. The following sections provide insights into the strain interpretation process for an instrumented concrete pile, commencing with installation, followed by concrete curing for cast-in-situ piles and soil consolidation/setup effects for driven piles, and finally, axial static/maintained load testing.

Table 1 comprises a series of instrumented concrete pile tests collated from the authors' records, the results of which are drawn upon in this paper to highlight various elements of the strain interpretation process. All piles were instrumented with vibrating wire strain gauges. In addition to pile type, length and diameter, the table also provides summary ground conditions, instrumentation type, strain gauge levels, and net change in strain and continuous measurements made between casting and axial load tests.

INSTALLATION AND CURING

Installation

For concrete piles, gauges are usually affixed to the pile reinforcement, either on site for cast-in-situ pile types, or in a casting yard for precast piles. As described in Flynn and McCabe (2021b), plunging of the reinforcement cage presents the greatest risk to the strain gauges for a cast-in-situ pile, whereas large driving stresses generated in precast piles can lead to cracking of the concrete, resulting in a loss of strain compatibility and erroneous strain output. As such, gauge readings taken after attachment to the cage and after installation is complete should be compared to assess if any damage has occurred.

Curing

The process of concrete curing may lead to the development of residual loads in cast-in-situ and driven piles between installation and load testing, while soil consolidation may also contribute in driven piles. A limited number of case histories have been reported in the literature and these are reviewed in Flynn and McCabe (2021b). Given the observed strain profiles, three approaches to interpreting residual loads in a cast-in-situ pile have been proposed. In this section, these methods are appraised using examples of curing behaviour obtained from the authors' records of instrumented driven cast-in-situ (DCIS) piles, the details of which are presented in Table 1.

The most basic method of interpretation, described by Kim et al. (2004), assumes that the net change in total strain between casting and conducting a load test is solely due to residual load. Designated Method 1 in this paper, this 'two-point' method is convenient as strain readings are only required immediately after casting and immediately prior to commencing a load test. The limitation of the simplified method lies in its inability to relate this 'lumped' change in strain to the component processes which occur prior to load testing.

To overcome this, the variation in strain and temperature over time can be obtained in a near-continuous manner using a datalogger (or an optical spectrum analyser for fibre optic sensors). Two interpretation methods based on such intermediate measurements have been proposed, with the main difference between them relating to the times at which residual load is assumed to develop:

- Pennington (1995) proposed calculating the change in temperature-corrected (i.e. mechanical) strain between peak temperature and load testing to represent the residual load in a cast-in-situ pile (Figure 1a), on the basis that the pile is in a stress-free state at peak temperature. This method is herein designated Method 2.
- Kim et al. (2011) propose a correction procedure, referred to herein Method 3, based on the assumption that residual loads are negligible at or near the head of the pile. By placing a set of strain gauges at this reference level, a strain profile which is independent of residual load can be obtained that can be compared to the profiles at the remaining sections of the pile. The instance at which a strain profile at a particular section begins to deviate from the trend

at the reference level is deemed to be the time at which residual loads begin to develop. The change in strain at each gauge level after this instance represents the strain due to residual load, as illustrated in Figure 1b. Note that the method does not require corrections for the effect of temperature on the measured strains.

Two of the test piles in Table 1 (D1 and P1) were constructed in mixed ground conditions, including layers of highly-compressible alluvial soils where negative skin friction was anticipated due to upfilling of ground levels, as well as excess pore pressures generated by tube installation. The remaining four piles (R1, R2, R3 and S1) were installed in uniform sand where downdrag loads were expected to be minimal. The net change in ε_{total} between casting and static load testing for the six piles is presented in Figure 2 (note that a positive sign convention has been used for compressive strains). It is apparent that tensile ε_{total} ($\approx$ 45 to 85 $\mu\varepsilon$) developed at the uppermost gauge level in all piles. Piles R1 to R3 and S1 in sand exhibited a near-constant tensile state throughout their embedded length. These tensile states imply that internal processes (e.g. internal restraint arising from shrinkage or swelling from moisture absorption) were influential. On the other hand, Piles D1 and P1 in layered soil demonstrated a reduction in tensile strain with depth, reaching a maximum compressive strain at the interface of the alluvial soils and underlying granular layer in which the piles were founded. These profiles resemble the classical distribution of dragload with depth with the neutral plane at the interface of the layers, suggesting that external processes (i.e. negative skin friction) had a dominant effect on these strains during curing. It is plausible that the larger compressive strain mobilised in Pile D1 in comparison to P1 is due to the greater thickness of soft soil (and hence dragload); however, the absence of continuous strain measurements during curing of Pile P1 precludes definitive conclusions in this regard.

To investigate how internal and external processes contribute to the development of residual loads in contrasting ground conditions, Piles D1 and S1 were connected to a datalogger for the entire curing period (approximately a fortnight, see Table 1), with measurements of strain and temperature logged at intervals of 15 minutes for the initial 24 hours and at hourly intervals thereafter. The resulting temperature and total (measured) strain profiles for Piles S1 and D1 are presented in Figures 3 and 4 respectively. The following points are noteworthy:

- At both sites, compressive total strains developed during initial set, with peak hydration temperatures occurring ~9 to 15 hours after casting, in keeping with previous findings summarised in Flynn and McCabe (2021b). Peak compressive total strains and temperatures were considerably greater at the uppermost gauge level in Pile S1 than at other levels, which was attributed to the larger cross-sectional area of the 0.6 m square pile cap in which the gauges were inadvertently cast.
- Compressive total strains subsequently reduced at all gauge levels after hydration temperatures had peaked and began to stabilise during the curing phase. The largest reduction in compressive strain occurred near the head of both test piles, in keeping with the observations of curing behaviour reported by Fellenius et al. (2009) and Kim et al. (2011).
- As the pile temperatures reached equilibrium, the total strains in Pile S1 were tensile throughout (Figure 3). In contrast, compressive strains began to develop in Pile D1 once again after 60-80 hours and continued to increase slowly for the remainder of the measurement period (Figure 4); this was attributed to the effect of dragload due to settlement in the alluvial soils induced by a combination of upfilling and dissipation of excess pore pressures generated by driving. These observations are again in keeping with previous research referenced in the companion paper.
- Cyclic variations in strain and temperature at the uppermost gauge level in Pile S1 were attributed to contraction and expansion of the pile cap due to the diurnal variation in air temperature. This effect could have been reduced or eliminated by ensuring that these gauges were within the pile (i.e. below ground level) rather than the pile cap.

Conversion of curing strains to load using Equation 1 is not a straightforward process, primarily because the pile modulus is time-dependent and hence is expected to be lower during the initial stages of curing when the concrete is in a semi-solid state (Neville and Brooks, 1987). The limited studies of residual load in the literature adopted a constant pile modulus based on empirical relationships with concrete strengths (Kim et al. 2004) or used direct measurements from the instrumentation in the subsequent static load test (Pennington, 1995; Siegel and McGillivary, 2009). For the examples presented herein, the authors have chosen the latter method for calculating residual load from the interpreted strains.

Figure 5 compares the derived residual load distributions for the two case histories using the aforementioned Methods 1 to 3, with Method 2 calculations based on temperature-corrected strain profiles using a coefficient of thermal expansion α = 12 $\mu\varepsilon$/ºC (as per Pennington (1995) and Farrell and Lawler (2008)). The addition of these residual loads to those measured during the subsequent static load test resulted in the load distributions (also shown in Figure 5) which increase with depth for Method 1 over a portion of the pile length and are greater than the applied load at the pile head for Method 2; see Figure 5b. These distributions would appear to be unrealistic, as the magnitude of displacement (>10 % of the pile diameter) induced during the static load test would be sufficient to reverse any negative shear stresses acting along the shaft of the piles.

On the basis of the above, Method 3 provides the most realistic load distributions, whereby the load reduces systematically with depth, with no erratic variations in load apparent. As such, this method has been advocated by Fellenius et al. (2009) and Kim et al. (2011) for interpreting residual load in cast-in-situ piles during curing. It is important to note, however, that these three methods have been developed from case histories involving the use of vibrating wire strain gauges to measure strain behaviour during curing. As highlighted by Flynn and McCabe (2021b), considerable uncertainty exists in the choice of an appropriate α-value for this gauge type, leading to contrasting strain profiles during curing. As such, further research into the curing behaviour of concrete piles using a combination of sensor types (e.g. VWSG and Distributed Fibre Optic Sensing or DFOS) is encouraged to provide greater insight into residual load development in cast-in-situ piles).

INTERPRETATION OF STATIC LOAD TEST STRAINS

The static load test is typically carried out once the pile concrete has reached sufficient compressive strength (typically 7 to 28 days, depending on the maximum applied load). Thermal strains may still persist if the hydration temperatures have yet to equalise. However, the relationship between time to peak temperature versus diameter, and time from peak temperature to 10 % excess temperature versus pile diameter squared in Flynn and McCabe (2021b) can be used to choose the earliest time for load tests such that their interpretation will not be complicated by thermal strains. At this stage, it is standard practice to re-zero the gauge readings so that any further changes in strain relate to the static load test only, with any residual loads mobilised during curing added to the load distribution at the end of the interpretation process. It should be noted that excess pore pressures due to pile driving, where relevant, may still be in existence once curing temperatures have decayed, and these may also impact upon the pile's performance under load.

The interpretation process commences with a review of the ε_{total} data. This is best performed in a visual manner initially by plotting the variation in (i) ε_{total} and applied load, P, with elapsed time, (ii) ε_{total} with pile head displacement and (iii) ε_{total} with P. An example of these plots is illustrated in Figure 6 for an array of four strain gauges at the uppermost level orientated at 90^{o} to each other (labelled 1 to 4 in a clockwise manner) in Pile D1. It is apparent that:

- The application of compression load results in a corresponding immediate increase in total strain in each gauge. Further gradual increases in strain occur during each load hold period due to creep within the concrete (Figure 6a).

- The strains in the four gauges begin to diverge from each other at an early stage in the load test due to pile bending, with the difference in strain continuing to increase as the applied load increased.
- Permanent tensile strains prevail when the pile was unloaded.

Thermal strains may also affect a concrete pile during a static load test, particularly in gauges near the ground surface where the influence of ambient air temperatures is greatest. These should be deducted from total strain to obtain mechanical strain using the same procedure as that for hydration temperatures during curing described previously.

Figure 7 illustrates an example of two malfunctioning gauges within a group of four at a given level in a 450mm diameter CFA pile (Pile C1) in layered soil; sudden reductions in strain occur during the hold period, possibly due to cracking of concrete or debonding of the gauge. Correction may not be possible in this instance, as a loss of strain compatibility is likely to have occurred, rendering the measured strains beyond this point unusable.

Creep

Creep is defined as permanent deformation of a material under constant load. For concrete, the process is considered long-term and hence is sometimes overlooked when performing short-duration instrumented concrete pile tests. Creep in concrete will increase as the applied stress reaches a greater proportion of the concrete's compressive strength (Neville and Brooks, 1987). This has greatest implications for preliminary concrete pile tests, where, unlike working pile load tests, the primary objective is to induce failure by subjecting the pile to a large compression load. As noted in Flynn and McCabe (2021b), pile testing specifications typically mandate that loads are held for an extended period of time (6 hours or greater) and such durations will undoubtedly promote the development of creep within a concrete pile, especially approaching the calculated ultimate pile resistance.

Figure 8a shows the variation in mechanical strain with time at the uppermost gauge level of a 600 mm diameter continuous flight auger (CFA) pile (Pile C2) during a maintained compression load test in accordance with the Institution of Civil Engineers (ICE) Specification for Piling and Embedded Retaining Walls or SPERW (ICE, 2017). The application of load at 13.4 hours resulted in an accompanying increase in strain (~100 με). However, the strain continued to increase (albeit at a significantly reduced rate) during the proceeding 3 hour hold period until the rate of settlement reduced to the minimum required by SPERW (resulting an additional 42 με). The strain behaviour during the next load increment was similar, with 100 με mobilised very quickly, followed by ~75 με more gradually during the 6.5 hour hold. Lam and Jefferis (2011) advocate that strains mobilised during the hold periods are due to creep within the concrete. The increases in strain immediately following application of load represent the true elastic responses which should be used to determine the elastic pile modulus; inclusion of creep in this process would lead to gross errors in the derived load at sections of the pile where creep was minimal. Separation of the mechanical strain into elastic and creep components is, at best, approximate, but is typically assumed to occur within 10 minutes after commencement of load application which is not instantaneous, taking several minutes to perform (Lam and Jefferis, 2011).

The elastic and creep strains for each load increment are assessed for each strain gauge using the procedure illustrated in Figure 8a, with the overall elastic response of the pile obtained by summing the individual elastic strain components for each stage (Lam and Jefferis, 2011; 2012). Figure 8b shows the resulting variation in mechanical (i.e. elastic plus creep) and cumulative elastic strains with time, where it is evident that creep accounts for a substantial portion of the mechanical strain at peak load. It is noteworthy that the elastic strain reduces to 0 με when the pile is fully unloaded at the end of the test; this is expected as the gauge in question was located close to the ground surface where residual loads are expected to be minimal (Kim et al. 2011). Interestingly, ignoring the effect of creep would result in a net compression strain of 500 με at the end of the test, implying that a large net compression load was present at the pile head after unloading, which is illogical. Hence, the correction for creep is warranted.

Pile bending

Following correction of the mechanical strains for creep, the next step is to assess the effect of pile bending during loading. Eccentricities inevitably occur during the application of axial load, resulting in bending which may increase significantly in the latter stages of a preliminary load test. The response of a pile to bending can be examined visually by plotting the measured strain with depth for a given orientation (e.g. 90^{o}, 180^{o}, 270^{o} and 360^{o}, when four gauges are placed per level). This procedure is illustrated in Figure 9a to c for cast-in-situ piles concrete piles at their maximum applied load in a maintained compression load test; commentary on each case is provided below.

The first example (Figure 9a) relates to the aforementioned 380 mm diameter DCIS pile in a highly-layered stratigraphy of low strength and stiffness (Pile P1). Variations in elastic strain were apparent at each gauge level, but particularly in the upper half of the pile where lateral fixity was reduced due to the presence of soft clay with bands of peat. The variation in elastic strain with depth for a 450 mm diameter continuous flight auger (CFA), designated Pile C1, is shown in Figure 9b. The variations in elastic strains at each level in this case are slightly lower, but could be considered less significant in relative terms given that larger average strains were mobilised; the only exception to this trend was at the uppermost gauge level within poorly-placed fill which allowed the pile head to rotate during loading due to the eccentricity in applied load during the test. Figure 9c represents a 1.5 m diameter bored pile (Pile F1) installed through Boulder Clay and into siltstone bedrock. The pile was double sleeved with outer and inner steel casings to the top of rock to minimise shaft resistance within the overburden during loading. The annulus between the casings was plugged with a weak cement-bentonite grout. The variation in elastic strain at maximum applied load shows significant variations at several gauge levels (including levels within the reduced-diameter rock socket), indicating that the pile was heavily influenced by bending throughout. The discrepancies in strain were most apparent at the uppermost gauge level, implying that the confinement provided by the weak bentonite grout within the annulus of the casings was insufficient to prevent lateral movements of the inner casing induced by eccentricities during loading.

In theory, the effect of pile bending in any axial plane can be minimised by placing only a pair of strain gauges at 180° to each other, as the average strain of the two strain readings will be representative of that at the pile centroid (Fellenius and Tan, 2012; Sinnreich, 2021). However, the impact of utilising an additional pair of gauges at 90° to the other pair is examined in Figures 10a to c for the uppermost gauge level of the three examples shown in Figure 9; these present the variation in average strain for each 180°–spaced gauge pair (i.e. 1-3 and 2-4), as well as all four gauges (1-2-3-4) during loading. For Pile P1, shown in Figure 10a, the averages of each pair and all four gauges are virtually identical throughout the load test. In the second example (Figure 10b), the average strains obtained from each gauge pair in Pile C1 begin to diverge from the average of the four gauges when the applied load is approximately one third of the maximum strain. This indicates that biaxial bending has developed due to the eccentricity in applied load occurring at a location between the axes of the strain gauge pairs. The divergence continues as the eccentricity in applied load exacerbates the bending moment. In Figure 10c, the lack of confinement within the double-sleeved casings of Pile F1 resulted in divergence in strain at < 10 % of the maximum applied load, although the rate of divergence began to slow as the applied load increased. Based on these examples, a case emerges for the use of four gauges at 90° where greatest bending is anticipated (crucial for modulus determination) and two gauges at 180° at other levels, in order to help minimise costs. However, selection of the depth along the pile at which a transition from four to two gauges is appropriate is by no means straight-forward and requires engineering judgement for the particular scenario under consideration.

If a gauge malfunctions during loading, it is standard practice to ignore the readings of the opposite gauge to prevent a biased estimate of average strain from the three remaining gauges (Sinnreich 2021). However, from inspection of Figures 10b and c, the remaining pair of strain gauges may have insufficient ability to compensate for biaxial bending when the eccentricity is located between the axes of the strain gauge pairs. This has significant implications for the derivation of the pile modulus using the uppermost gauge level (as described in the following section), as the examples demonstrate that this level is most vulnerable to bending effects. Such effects may be alleviated to some extent by the use of steel casing to enhance the pile's flexural resistance between the cap and the first gauge level (as reported by Lam and Jefferis, 2011). The examples in Figures 9 and 10 demonstrate that the majority of bending occurs near the pile head, primarily due to poor lateral confinement under axial load (either from the surrounding soil of poor strength or the use of weak bentonite grout within the annulus of the double-sleeved casings), with discrepancies in strain output significantly reducing with depth.

Pile modulus

The derivation of the pile modulus is arguably the most challenging stage in the interpretation process due to the non-linear behaviour of concrete, and the use of an erroneous modulus can result in gross errors in the interpreted load distribution. Various methods for deriving the pile modulus have been proposed and readers are referred to a comprehensive review of these methods by Lam and Jefferis (2011). Table 2 (adapted from Lam and Jefferis, 2011) summarises the key equations and parameters of each method.

The pile modulus can be ascertained using (i) direct methods based on the strain readings from the pile instrumentation during loading, e.g. tangent modulus (Fellenius, 1989), secant modulus (Lam and Jefferis, 2011) and time-dependent secant modulus (Lehane et al., 2003) methods, or (ii) indirect methods whereby the pile modulus is assumed to correspond to laboratory measurements of concrete modulus (using instrumented concrete specimens or dummy piles) or by empirical relationships with compressive strength presented in design codes (e.g. CEN, 2004).

The popularity of pile modulus interpretation methods was appraised by the authors using the pile test database presented in Flynn and McCabe (2021b). Unfortunately, 34 % of sites in the database did not report the pile modulus method used and consequently, a reduced database of 77 case histories is presented in Table 3. Of these, 70 % of the studies derived the pile modulus using direct methods, with the tangent and secant methods equally represented. The transformed area, uncorrected area and dummy pile indirect methods accounted for only 15, 12 and 3 of the sites in the database, respectively; this outcome reflects the poor reliability of these methods in estimating the pile modulus (and hence load) in comparison to the direct methods, as reported by several authors (Patel, 2010; Siegel, 2010; Lam and Jefferis, 2011; Sahajda, 2013). Their use as the primary method for derivation of the pile modulus is therefore discouraged.

For direct methods, the primary purpose of the uppermost gauge level is to serve as a direct calibration of strain with the applied load. As such, this level should be placed as close to the head of the pile as possible in order to minimise intervening shaft resistance which would inhibit comparability; further guidance on this is presented in Flynn and McCabe (2021b). Particular attention should be given to the dimensions of the pile cap, as an enlarged cap area relative to the pile may lead to end-bearing resistance on the underside of the pile cap during loading and unrepresentative strains.

As noted previously, the modulus of concrete is a non-linear (second order) function of strain. Fellenius (1989), however, noted that the relationship between tangent modulus $E_{pile,tangent}$ = $\Delta\sigma/\Delta\varepsilon_{elastic}$ (where $\Delta\sigma$ and $\Delta\varepsilon_{elastic}$ are the respective changes in stress and elastic strain between each load increment) and elastic strain becomes linear when the shaft resistance is fully mobilised.

By means of linear regression, the relationship between $E_{pile,tangent}$ and strain can be obtained using Equation 4:

$$E_{pile,tangent} = A_{tangent}\varepsilon_{elastic} + B_{tangent} \quad (4)$$

where $A_{tangent}$ is the slope of the tangent modulus line and $B_{tangent}$ is the $E_{pile,tangent}$–axis intercept. These constants are subsequently used to obtain the equivalent secant modulus $E_{pile,secant}$, as follows:

$$E_{pile,secant} = 0.5A_{tangent}\varepsilon_{elastic} + B_{tangent} \quad (5)$$

In the secant method, the pile modulus is determined directly from the measured stress-strain response using the secant slope, as follows:

$$E_{pile,secant} = P/A_{pile}\varepsilon_{elastic} \quad (6)$$

The resulting relationship between $E_{pile,secant}$ and $\varepsilon_{elastic}$ is ascertained by fitting an appropriate trendline (e.g. polynomial, exponential, or logarithmic) to the data.

For precast concrete piles, the A_{pile} term in Equation 1 is known in advance of the load test (provided no breakages occur during driving). In the case of cast-in-situ piles, the true diameter (and hence area) of the pile may differ from the nominal diameter due to the complex interaction between the fluid concrete and surrounding ground. In most instances, extraction of the test pile will be prohibitive for both cost and health and safety reasons; only 3 of the case histories in Table 3 report an as-constructed diameter for cast-in-situ variants. As such (based on the case histories collated in Table 3), it is common to assume that that the pile diameter corresponds to the diameter of the auger for CFA and drilled displacement piles, the outer diameter of the casing and/or drilling tool for bored piles and the diameter of the sacrificial driving shoe for DCIS piles. Ideally, the sensitivities in shaft and base resistances to the assumed pile diameter should also be assessed, as demonstrated by Flynn and McCabe (2021a) for DCIS piles. Nonetheless, measurement of the pile cross-sectional area is not strictly necessary, as the lumped $E_{pile}A_{pile}$ term (known as axial rigidity

(Marinucci et al. (2021)) can be determined from measured load-strain response. Lam and Jefferis (2011) provide guidance on interpreting axial rigidity for a composite pile (e.g. a bored pile with a reduced-diameter rock socket). Further commentary on the merits of comparing the moduli or axial rigidities derived using the secant and tangent methods as part of the interpretation process is given by Fellenius (2012) and Lam and Jefferis (2012).

Figure 11 shows a comparison of the secant and tangent methods applied to a 380 mm diameter DCIS pile (Pile D1). The tangent axial rigidity ($E_{pile,tangent}A_{pile}$) is plotted against elastic strain in Figure 11a for all gauge levels during loading. A near-linear variation in $E_{pile,tangent}A_{pile}$ is apparent for the uppermost gauge level (1.3 m) throughout the test, whereas the remaining gauges become linear after approximately 250 $\mu\varepsilon$, as the shaft resistance becomes fully mobilised along the embedded pile length (note that shaft resistance also results in the data plotting above the trendline in Figure 11a, as the true load at these levels is less than the applied load). A linear trendline has been fitted to the data for 1.3 m and the equivalent strain-dependent $E_{pile,secant}A_{pile}$ obtained using Equations 4 and 5. The resulting relationship is illustrated in Figure 11b, together with the data ascertained by direct calculation of the secant axial rigidity using Equation 6. The methods show reasonable agreement, although some variability is apparent for the secant method, as the axial rigidity was deduced directly from the data, rather than by linear regression. The range of $E_{pile}A_{pile}$ values are consistent with a modulus of 26 to 28 GPa for a nominal diameter of 380 mm, which is plausible for a concrete pile tested approximately 13 days after casting.

Figure 12a illustrates two examples (using Piles P1 and S1) of how multiple unload-reload cycles (with unequal load increments) complicate the tangent and secant rigidity derivations. In these scenarios, the back-figured rigidities for the uppermost gauge levels exhibited more variability in comparison to Figure 11, with the tangent rigidity being particularly sensitive to changes in strain (due to the use of differentiation, as noted by Fellenius (2012)). Unloading will induce additional residual loads which may affect the response of the pile, as illustrated by the higher tangent rigidities in the proceeding cycle. As such, the $E_{pile}A_{pile}$-$\varepsilon_{elastic}$ relationship must be considered separately for each cycle, rather than deduced from a continuous dataset for the entire test. However, load increments often differ for the reload phase, with ICE SPERW, for example, specifying an initial reload increment corresponding to the peak load from the previous cycle, followed by two additional increments and then unloading. As shown in Figure 12, there are only three datapoints available with which to determine the rigidity for the second cycle and these are located within a relatively narrow strain range (100 to 150 με and 300 to 450 με in Figure 12a and b, respectively). Furthermore, the strains at the remaining levels are likely to be outside of the lower end of this range and the resulting extrapolation of rigidity may introduce further errors into the interpretation process. The axial rigidity is shown to increase with strain for the third load cycle in Figure 12b; this phenomenon has been experienced by the authors on occasion, and has also been noted in the literature (e.g. Fellenius 2020). It is attributed to post-peak reductions in shaft resistance at this level (2.5 mbgl) arising from the two load cycles and may also indicate that some shaft resistance was present between the pile head and the gauge level. Several authors (Lam and Jefferis 2011, 2012; Fellenius 2012) have questioned the need to carry out such loading cycles in instrumented load tests and the examples presented herein serve to highlight the associated interpretation difficulties that may arise when these are performed.

The effect of bending on the mobilised elastic strain during loading can be significant, leading to further difficulties in the interpretation of pile rigidity. Figure 13 illustrates the secant axial rigidity - elastic strain response obtained from the uppermost gauge level of the example presented in Figure 10b (where bending was significant during the test). A divergence in derived axial rigidity from each of the two gauge pairs (1-3 and 2-4) develops when $\varepsilon_{elastic}$ exceeds 200 με, with large increases in rigidity derived from the first gauge pair (1-3) most apparent. The remaining pair (2-4) exhibits a more realistic response, with $E_{pile}A_{pile}$ reducing with $\varepsilon_{elastic}$ at a gradual rate. It is likely that the rigidity obtained using all four gauges is biased to some extent due to the behaviour of the first gauge pair.

Load Distribution

The final step in the interpretation process is to convert the elastic strains to pile loads. The load at each level is calculated using Equation 1 in conjunction with the strain-dependent secant modulus at the uppermost gauge level. First, the variation in average strain with applied load should be plotted for each gauge level, as shown in Figure 14 for Piles S1 and P1. The load-strain response at all levels become parallel to one another in the latter stages of the test on Pile S1 in Figure 14a, which indicates that the shaft resistance was fully mobilised. This is not the case for the Pile P1 dataset in Figure 14b, however, where the resistances continue to increase and show no sign of reaching peak values at the maximum applied load.

Where residual loads were measured during the curing process, these should be added to obtain the true load distribution (Selemetas and Standing, 2017). The resulting loads should be plotted with depth as illustrated in Figure 15a for Pile D1. The plots should be scrutinized for signs of abnormal variations, such as the increase in load between 3.5 m and 6.5 m in Figure 15a. In this instance, the strain gauges at 3.5 m were located within a section of the pile shaft where a layer of very soft peat was encountered during the ground investigation and it was suspected that significant concrete overbreak occurred at this depth during concreting, resulting in an enlarged pile cross-section. As a result, the axial rigidity was under-estimated, leading to an apparent shedding of load across this layer inconsistent with its very soft to soft undrained shear strength. Therefore, these readings were ignored and the estimated true distribution is illustrated by the dashed lines in Figure 15a.

Shaft resistance

The shear stress τ_s between two successive gauge levels is derived from the load distribution using Equation 6:

$$\tau_s = \frac{\Delta Q_s}{\pi D_s L_i} \qquad (6)$$

where ΔQ_s and L_i are the change in shaft load and the distance between successive gauge levels, respectively, and D_s is the pile shaft diameter. Strain gauges enable the change in load between successive levels to be determined and hence the shear stress across this distance is considered to represent of the average shear stress, rather than a local measurement obtainable using surface stress transducers (e.g. Lehane et al. 2012; Royston et al. 2021). As such, plotting the distribution of shear stress with depth as single datapoints at the midpoint between gauges and joined by a line can be deceptive if the distance between levels is large. Presentation of the data as illustrated in Figure 15b, i.e. as constant values between gauge levels, may be more appropriate in this instance.

Base resistance

The lowermost level of discrete-type strain gauges should ideally be placed within 250 mm of the base of the test pile to enable accurate estimation of the base resistance during loading. However, the lowermost gauge level of the piles in the database of Flynn and McCabe (2021b) ranged from 0 to 7.9 m and hence, extrapolation is typically relied upon to derive the base resistance.

Figure 16 shows the base resistance-displacement response of Pile C1 derived by extrapolating the load distribution linearly from the lowermost gauge level (~200 mm from the base). The next lowest gauge level was situated 1.6 m from the base; extrapolation from this level (see inset) results in the base resistance being grossly over-estimated. It is therefore crucial that strain gauges are placed as close to the base as possible in order to minimise errors associated with extrapolation. Increased use of DFOS systems in the future, rather than discrete strain measurement systems, will enable more accurate assessments of pile base loads, obviating the need for extrapolation.

CONCLUSIONS

The interpretation of data from an instrumented concrete pile is not a simple process, with factors such as installation and curing effects, creep, bending and testing procedures influencing the measured strains. Various techniques advocated in the literature for interpreting data from instrumented concrete piles have been demonstrated and appraised with the help of case histories, in an attempt to reduce such uncertainties for practitioners. Key conclusions from this process included:

- Assessment of residual loads in cast-in-situ piles during curing is enhanced by continuous monitoring of strain and temperature during this period. Uncertainties in correction for thermal-related effects hampers this assessment when using vibrating wire strain gauges, with fibre optic sensors expected to provide more definitive interpretations.
- Prolonged hold periods promote the development of irreversible creep strains within the concrete, which must be deducted from total strains to derive elastic strains.
- The effects of bending on the measured strains are most prevalent at the upper sections of the pile (where confinement from the soil may be reduced). However, these effects can be mitigated to some extent by using four gauges at the uppermost level.
- The strain-dependent pile modulus should be derived using the creep-corrected strain data from the uppermost gauge level in conjunction with the tangent and secant modulus methods.
- Unload-reload cycles have an unhelpful impact on the interpretation process and should be discouraged for instrumented pile tests.
- Discrete-type strain gauges (i.e. electrical resistance, vibrating wire and fibre Bragg grating) should be placed as close as possible to the base to minimise errors due to extrapolation in calculating the base resistance.

It is hoped that this paper, in conjunction with the companion paper by Flynn and McCabe (2021b), will support an increased uptake and a more meaningful interpretation of instrumented load tests on preliminary piles.

ACKNOWLEDGEMENTS

The first author was sponsored by the College of Engineering and Informatics Fellowship and University Foundation Bursary during his doctoral studies at NUI Galway. The views expressed in this paper are solely the opinions of the authors and do not represent the views of AGL Consulting.

REFERENCES

Abdlrahem MA and El Naggar MH (2020) Axial performance of micropile groups in cohesionless soil from full-scale tests. Canadian Geotechnical Journal 57(7): 1006–1024.

Abu-Farsakh M, Nafiul Haque M, Tavera E and Zhang Z (2017) Evaluation of pile setup from Osterberg Cell load tests and its cost-benefit analysis. Transportation Research Record: Journal of the Transportation Research Board, 2656, 61–70.

Altee A, Fellenius BH and Evgin E (1992) Axial load transfer for piles in sand. I. Tests on an instrumented precast pile. Canadian Geotechnical Journal 29(1): 11–20.

Avasarala S, Mummaneni S, Vemula V and Putcha S (2017). Case study: load transfer analysis on an instrumented augercast pile using EDC strain gauges and Geokon rebar strainmeters. In Pr*oceedings of DFI-PFSF Piled Foundations & Ground Improvement Technology for the Modern Building and Infrastructure Sector, Melbourne, Australia*, pp. 356–366.

Baker C (1991) Prediction and performance of drilled shafts constructed under slurry. In *Proceedings of the 16th DFI Annual Conference, Chicago, Illinois, USA*, pp. 155–172.

Bersan S, Bergamo O, Palmieri L, Schenato L and Simonini P (2018) Distributed strain measurements in a CFA pile using high spatial resolution fibre optics sensor. Engineering Structures 160: 554–565.

CEN (Comité Européen de Normalisation) (2004) Eurocode 2: Design of Concrete Structures – Part 1-1: General Rules and Rules for Buildings. EN 1992-1-1-2004. CEN, Brussels, Belgium.

Chen CS and Hiew LC (2006) Performance of bored piles with difference construction methods. Proceedings of the Institution of Civil Engineers – Geotechnical Engineering 159(3): 227–232

Chen Q, Nafiul Haue M, Abu-Farsakh M and Fernandez BA (2014) Field investigation of pile setup in mixed soil. Geotechnical Testing Journal 37(2): 1–14.

Cunningham JN, Struedlein AW and Castañeda MA (2011) Uplift micropile load transfer in unsaturated Missoula flood deposits. In *Proceedings of the 36th Annual Conference on Deep Foundations, Boston, MA, USA*, pp. 629–636.

Drbe OFE and El Naggar MH (2015) Axial monotonic and cyclic compression behaviour of hollow-bar micropiles. Canadian Geotechnical Journal 52(4): 426–441.

Farrell ER and Lawler M (2008) CFA pile behaviour in very stiff lodgement till. Proceedings of the Institution of Civil Engineers – Geotechnical Engineering 161(1): 49–57.

Fellenius BH (1989) Tangent modulus of piles determined from strain data. In *Proceedings of the 1989 Foundation Congress,* ASCE, Renton, USA, Volume 1, pp. 500–510.

Fellenius BH (2012) Discussion of "Critical assessment of pile modulus methods". Canadian Geotechnical Journal 49(5): 614–621.

Fellenius BH (2020) The tangent stiffness uncertainty in strain-hardening and strain-softening soil. Geotechnical Engineering Journal of the SEAGS & AGSSEA 51(1): 89–93.

Fellenius BH and Nguyen MH (2013) Large diameter long bored piles in the Mekong delta. International Journal of Geoengineering Case Histories 2(3): 196–207.

Fellenius BH and Ruban T (2020) Analysis of strain-gage records from a static loading test on a CFA pile. DFI Journal 14(1): 39–44.

Fellenius BH and Tan SA (2010) Combination of bidirectional-cell test and conventional head-down test. In *The Art of Foundation Engineering Practice, GSP 198*, pp. 240–259.

Fellenius BH and Tan SA (2012) Analysis of bidirectional-cell tests for Icon Condominiums, Singapore. In *Proceedings of the 9th International Conference on Deep Foundations and Testing – IS Kanazawa, Kanazawa, Japan*, pp. 725–733.

Fellenius BH and Terceros M (2014) Response to load for four different types of bored piles. In *Proceedings of the DFI/EFFC 11th International Conference on Piling and Deep Foundations, Stockholm, Sweden*, pp. 1–21.

Flynn KN (2014) Experimental investigations of driven cast-in-situ piles. Ph.D thesis. Department of Civil Engineering, National University of Ireland Galway, Galway, Ireland.

Flynn KN and McCabe BA (2021a) Applicability of CPT capacity prediction methods to driven cast-in-situ piles in granular soil. Journal of Geotechnical and Geoenvironmental Engineering 147(2), 04020170-1.

Flynn KN and McCabe BA (2021b) Instrumented concrete pile tests – Part 1: instrumentation and procedures. Proceedings of the Institution of Civil Engineers – Geotechnical Engineering. Submitted.

Gajjar RH, Basarkar YC and Dewaikar DM (2005) Analytical and field estimates of shaft resistance in socketed piles: Bandra-Worli Sea Link, Mumbai. In *Proceedings of the 30th Annual Conference on Deep Foundations, Chicago, Illinois, USA*, pp. 303–313.

Galbraith AP (2011) Design and performance of deep foundations in Ireland. Ph.D thesis. Department of Civil, Structural and Environmental Engineering, Trinity College Dublin, Ireland.

Gavin KG, Cadogan D and Casey P (2009) Shaft capacity of continuous flight auger piles in sand. Journal of Geotechnical and Geoenvironmental Engineering 135(6): 790–798.

Gavin KG, Cadogan D and Twomey L (2008) Axial resistance of CFA piles in Dublin Boulder Clay. Proceedings of the Institution of Civil Engineers – Geotechnical Engineering 161(4): 171–180.

Glisic B, Inaudi D and Nan C (2002) Pile monitoring with fibre optic sensors during axial compression, pullout, and flexure tests. Transportation Research Record: Journal of the Transportation Research Board 1808: 11–20.

Gura NP, McGettigan ME and Archabal RA (2007) Engineering foundation support for Las Vegas Strip's tallest hotel casino. In *Proceedings of the 32nd DFI Annual Conference on Deep Foundations, Colorado Springs, CO, USA*, pp. 1–10.

Hai NM and Dao DH (2013) Non-conventional pile loading tests in Vietnam. In *Proceedings of the 18th International Conference on Soil Mechanics and Geotechnical Engineering, Paris, France*, pp. 2747– 2750.

Holman TP (2009) High capacity micropiles in Wissahickon Schist bedrock. In *Contemporary Topics in Deep Foundations, Geotechnical Special Publication No. GSP185, Orlando, FL, USA*, pp. 103–110.

Holman TP, Papthanasiou Y, Gallagher MJ and Khoury M (2007) Piled raft floats on moraine. In *Proceedings of the 32nd DFI Annual Conference on Deep Foundations, Colorado Springs, CO, USA*, pp. 1–12.

ICE (2017) *Specification for Piling and Embedded Retaining Walls (SPERW), 3rd Edition*. ICE, London, United Kingdom.

Ismael NF (2001) Axial load tests on bored piles and pile groups in cemented sands. Journal of Geotechnical and Geoenviromental Engineering 127(9): 766–773.

Ismael NF and Farraj K (2014) Analysis of load transfer along large diameter bored piles in very dense sands. In *Proceedings of the 39th DFI Annual Conference on Deep Foundations, Atlanta, GA, USA*, pp. 153–159.

Jacobson JR, Camp WM and Siegel TC (2011) Continuous flight auger piles in the Blue Ridge: a case study using instrumentation in pile design. In *Proceedings of the 36th Annual Conference on Deep Foundations, Boston, MA, USA*, pp. 315–324.

Justason MD, Mullins G, Robertson DT and Knight WF (1998) A comparison of static and statnamic load tests in sand: a case study of the Bayou Chico Bridge in Pensacola, Florida. In *Proceedings of the 7th International Conference & Exhibition on Piling and Deep Foundations, Vienna, Austria*, pp. 187–194.

Kania JG and Katoka Sørensen K (2018) A static pile load test on a bored pile instrumented with distributed fibre optic sensors. In *Proceedings of the International Symposium on Field Measurements in Geomechanics (FMGM 2018), Rio de Janeiro, Brazil*, pp. 1–9.

Khan, MK, El Naggar MH and Elkasabgy M (2008) Compression testing and analysis of drilled concrete taped piles in cohesive-friction soil. Canadian Geotechnical Journal 45(3): 377–392.

Kim M-G, Cavusoglu E, O'Neill MW, Roberts T and Yin S (2004) Residual load development in ACIP piles in a bridge foundation. In *Geosupport Conference 2004, Orlando, Florida, USA*, pp. 223–235.

Kim S-R, Chung S-G and Fellenius BH (2011) Distribution of residual load and true shaft resistance for a driven instrumented test pile. Canadian Geotechnical Journal 48(4): 583–598.

Kou H-L, Chu J, Guo W and Zhang M-Y (2016) Field study of residual forces developed in pre-stressed high-strength concrete (PHC) pipe piles. Canadian Geotechnical Journal 53(4): 696–707.

Krishnan S and Kai LS (2006) A novel approach to the performance evaluation of driven prestressed concrete piles and bored cast-in-place piles. In *Proceedings of the DFI/EFFC 10*th *International Conference on Piling and Deep Foundations, Amsterdam, Netherlands*, pp. 718–726.

Krishnendu M (2015) Instrumented pile load tests on ACIP piles for a real estate project in Kolkata – a case study. In *Proceedings of the 6*th *Conference on Deep Foundation Technologies for Infrastructure Development in India*, pp. 192–201.

Lam C and Jefferis SA (2011) Critical assessment of pile modulus determination methods. Canadian Geotechnical Journal 48(10): 1433-1448.

Lam C and Jefferis (2012) Reply to the discussion by Fellenius on "Critical assessment of pile modulus determination methods". Canadian Geotechnical Journal 49(5): 622–629.

Lam C, Jefferis SA, Suckling TP and Troughton VM (2015) Effects of polymer and bentonite support fluids on the performance of bored piles. Soils and Foundations 55(6): 1487–1500.

Lee W, Lee W-J, Lee S-B and Salgado R (2004) Measurement of pile load transfer using the Fiber Bragg Grating sensor system. Canadian Geotechnical Journal 41(6): 1222–1232.

Lehane BM, Pennington S and Clarke S (2003) Jacked end-bearing piles in the soft alluvial sediments of Perth. Australian Geomechanics Journal 38(3): 123-135.

Li B and Ruban AF (2009) Static axial load test on strain gauge instrumented concrete pile. In *Proceedings of GeoHalifax 2009*, pp. 227-233.

Lim A, Kwanda A and Rahardjo PP (2013) The study of t-z and q-z curves on bored pile based on the results of instrumented pile load test in medium and stiff clays. In *Proceedings of Pile 2013*, pp. 1 to 5.

Ling Z, Wang W, Wu J, Huang M and Yuan J (2019) Shaft resistance of pre-bored precast piles in Shanghai clay. Proceedings of the Institution of Civil Engineers – Geotechnical Engineering 172(2): 228–242.

Liu J, Zhang Z, Yu F and Yang Q (2013) Termination criteria for jacked precast high-strength prestressed concrete pipe piles. Proceedings of the Institution of Civil Engineers – Geotechnical Engineering 166(3): 268–279.

Marinucci A, Moghaddam RB and NeSmith WM (2021) Full-scale load testing and extraction of augered cast-in-place (ACIP) piles in Central Florida. DFI Journal 15(1): 1–21.

Mohamad H, Tee BP, Chong MF and Ang KA (2017) Investigation of shaft friction mechanisms of bored piles through distributed optical fibre strain sensing. In *Proceedings of the 19th International Conference on Soil Mechanics and Foundation Engineering, Seoul, South Korea*, pp. 2829–2932.

Muchard M (2006) Statnamic load testing of high capacity marine foundations. In *Proceedings of the DFI Annual Conference*, 2005.

Muthukkumaran K, Sundaravadivelu R and Gandhi SR (2007) Effect of dredging and axial load on a berthing structure. International Journal of Geoengineering Case Histories 1(2): 73–88.

Neville A and Brooks J (1987) *Concrete technology*. Longman Group, Harlow, United Kingdom.

Nguyen MH and Fellenius BH (2015) Bidirectional cell tests on not-grouted and grouted large-diameter bored piles. Journal of Geo-Engineering Sciences 2(3-4): 105–117.

Nguyen MH and Fellenius, BH (2014) Bidirectional-cell tests on two 70m long bored piles in Vietnam. In *GeoInstitute Geo Congress 2014*, pp. 482–496.

Nie R, Leng W, Yang Q and Chen YF (2016) An improved instrumentation method for PHC piles. Proceedings of the Institution of Civil Engineers – Geotechnical Engineering 169(6): 494–508.

Omer JR (1998) Numerical analysis of test pile data from instrumented large diameter bored piles formed in Keuper Marl (Mercia Mudstone). PhD thesis. Department of Civil Engineering, University of Glamorgan.

Patel D, Williamson M, Troughton V and Pennington M (2010) Instrumented underream pile test in London Clay constructed using new Stent underream tool. In *Proceedings of the DFI and EFFC 11th International Conference on Geotechnical Challenges in Urban Regeneration, London, UK.*

Pelecanos L, Soga K, Chunge MPM, Ouyong Y, Kwan V, Kechavarzi C and Nicholson D (2017) Distributed fibre-optic monitoring of an Osterberg-cell pile test in London. Géotechnique Letters 7(2): 152–160.

Pelecanos L, Soga K, Elshafie MZ, De Battista N, Kechavarzi C, Gue CY, Ouyang Y and Seo HJ (2018) Distributed fiber optic sensing of axially loaded bored piles. Journal of Geotechnical and Geoenvironmental Engineering: 144(3), 04017122-1 to 16.

Pennington DS (1995) Cracked? Exploring post-construction evidence in the interpretation of trial pile data. Proceedings of the Institution of Civil Engineers – Geotechnical Engineering 113(2): 132–143.

Puller DJ, Corbet SP and Patterson D (2002) Design of bored piles in chalk at the new Medway crossing based on instrumented load tests. In *Proceedings of the 9th International Conference on Piling and Deep Foundations, Nice, France*, pp. 569–573.

Riker RE and Fellenius BH (1992) A comparison of static and dynamic pile test results. In *Proceedings of the 4th International Conference on the Application of Stress-Wave Theory of Piles*, pp. 143–152.

Royston R, Sheil BB and Byrne BW (2021) Monitoring the construction of a large-diameter caisson in sand. Proceedings of the Institution of Civil Engineers – Geotechnical Engineering. In press. DOI: 10.1680/jgeen.19.00266.

Russo G (2004) Full-scale load tests on instrumented micropiles. Proceedings of the Institution of Civil Engineers – Geotechnical Engineering 157(3): 127–135.

Sahajda K (2013) Nonlinearity of concrete modulus and its influence on the interpretation of instrumented pile load tests. In *Proceedings of the Conference on Concrete Structures in Urban Areas, Wroclaw, Poland*, pp. 1–10.

Saglamer A, Elif Y, Muge I and Orhan I (2001) Load test on a large diameter instrumented bored pile. In *Proceedings of the 15th International Conference on Soil Mechanics and Geotechnical Engineering, Istanbul, Turkey*, pp. 999–1002.

Selemetas D and Standing JR (2017) Response of full-scale piles to EPBM tunnelling in London Clay. Géotechnique 67(9): 823–836.

Seo H, Prezzi M and Salgado R (2013) Instrumented static load test on rock-socketed micropile. Journal of Geotechnical and Geoenvironmental Engineering 139(12): 2037–2047.

Shahien MM and El Naggar HM (2015) Analysis of three axial load tests on large bored grouted deep foundations. In *Proceedings of the 40th DFI Annual Conference on Deep Foundations, Oakland, CA, USA*, pp. 311–320.

Siegel TC (2010) Load testing and interpretation of instrumented augered cast-in-place piles. DFI Journal 4(2): 65–71.

Siegel TC and McGillivray A (2009) Interpreted residual load in an augered cast-in-place pile. In *Proceedings of the Deep Foundations Institute Annual Conference, Kansas City, MO, USA*, pp. 1–10.

Sienko R, Bednarski L,Kanty P and Howiacki T (2018) Application of distributed optical fibre sensor for strain and temperature monitoring within continuous flight auger columns. IOP Conference Series: Earth and Environmental Science 221, 012006.

Sinnreich J (2021) Optimizing the arrangement of strain gauges in pile load testing. Geotechnical Testing Journal 44(5), GTJ20200033

Vipulanandan C, Vembu K and Brettmann T (2009) Load displacement behavior of ACIP piles in cohesive soils. In *Contemporary Topics in Deep Foundations, Geotechnical Special Publication No. GSP185, Orlando, FL, USA*, pp. 103–110.

Vipulanandan C, Vembu K and Guvener O (2012) Monitoring auger cast in place pile construction and testing in hard clay. In *Proceedings of the 37th DFI Annual Conference on Deep Foundations, Houston, TX, USA*, pp. 67–76.

Wang Y, Sang S, Zhang M, Bai Z and Su L (2021) Investigation on in-situ test of penetration characteristics of open and closed PHC pipe piles. Soils and Foundations, In press, displacehttps://doi.org/10.1016/j.sandf.2021.06.003

Wilkinson PD and Butterworth CS (2006) Report on an instrumented continuous flight auger test pile at Ascot. In *Proceedings of the DFI/EFFC 10th International Conference on Piling and Deep Foundations, Amsterdam, The Netherlands*, pp. 790–795.

Zhan C and Yin J-H (2000) Field static load tests on drilled shaft founded on or socketed into rock. Canadian Geotechnical Journal 37(6): 1283–1294.

Notation

$A_{tangent}$, $B_{tangent}$ = regression parameters for tangent method

A_{pile} = pile cross-sectional area

D = pile diameter

D_s = pile shaft diameter

E_{pile} = pile modulus

$E_{pile,secant}$ = secant pile modulus

$E_{pile,tangent}$ = tangent pile modulus

$E_{pile}A_{pile}$ = pile axial rigidity

$E_{pile}A_{secant}$ = secant axial rigidity

$E_{pile}A_{tangent}$ = tangent axial rigidity

GF_{VW} = vibration wire gauge factor

L_i = distance between successive gauges

P = load

T = temperature

$T_{ambient}$ = ambient temperature

T_{peak} = peak hydration temperature

ΔQ_s= change in shaft load

$\Delta\sigma$ = change in stress

$\Delta\varepsilon_{elastic}$ = change in elastic strain

α = coefficient of thermal expansion

ε = total strain

ε_{creep} = creep strain

$\varepsilon_{elastic}$ = elastic strain

$\varepsilon_{thermal}$ = thermal strain

ε_{total} = total (measured) strain

τ_s = shear stress

List of Table Captions

Table 1. Database of instrumented strain piles from authors' records.

Table 2. Pile modulus interpretation methods (adapted from Lam and Jefferis, 2011).

Table 3. Pile test database with pile modulus interpretation methods.

List of Figure Captions

Figure 1. Interpretation of residual loads during curing using continuous strain measurements – (a) Method 1 and (b) Method 2

Figure 2. Net change in total strain between casting and commencing static load test for selected DCIS piles in Table 1

Figure 3. Variation with time after casting of (a) temperature and (b) strain – Pile S1 in uniform medium dense to dense sand

Figure 4. Variation with time after casting of (a) temperature and (b) strain – Pile D1 in layered soil

Figure 5. Interpreted residual load distribution during curing and ultimate load distribution during static load testing for (a) Pile S1 in uniform sand and (b) Pile D1 in layered soil

Figure 6. Variation of (a) strain and applied load with time, (b) strain with displacement and (c) strain with applied load during static compression load test at uppermost gauge level of Pile D1 in layered soil

Figure 7. Example of malfunctioning strain gauges during static compression load test on Pile C1 in layered soil

Figure 8. (a) Elastic and creep strains during maintained compression load test and (b) measured and creep-corrected strain response of Pile C2 in uniform sand

Figure 9. Examples of strain distribution with depth for (a) Pile P1 in layered soil, (b) Pile C2 in layered soil and (c) Pile F1 in rock with double sleeved casings in overburden

Figure 10. Effect of pile bending on average strains during loading for (a) Pile P1 in layered soil, (b) Pile C2 in layered soil and (c) Pile F1 in rock with double sleeved casings in overburden

Figure 11. Variation with elastic strain of (a) tangent axial rigidity and (b) secant axial rigidity for Pile P1 in layered soil

Figure 12. Influence on tangent and secant axial rigidities of (a) multiple load cycles for Pile P1 in layered soil and (b) strain hardening during loading of Pile S1 in uniform sand

Figure 13. Effect of pile bending on secant pile axial rigidity of Pile C1 in layered soil

Figure 14. Variation in average elastic strain at each gauge level with applied load, highlighting (a) full mobilisation of shaft resistance for Pile S1 in uniform sand and (b) partial mobilisation of shaft resistance for Pile P1 in layered soil

Figure 15. Variation with depth of (a) load and (b) shear stress for Pile D1 in layered soil

Figure 16. Effect of gauge distance from pile base on extrapolation for determining base resistance during loading of Pile C1 in layered soil

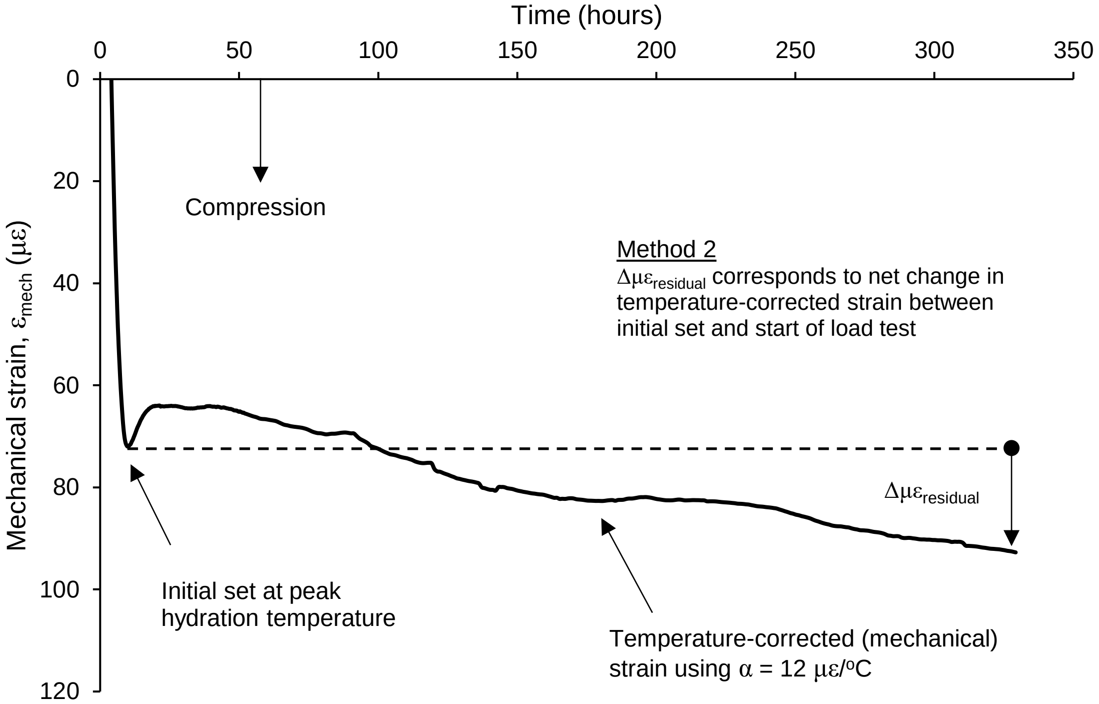

(a)

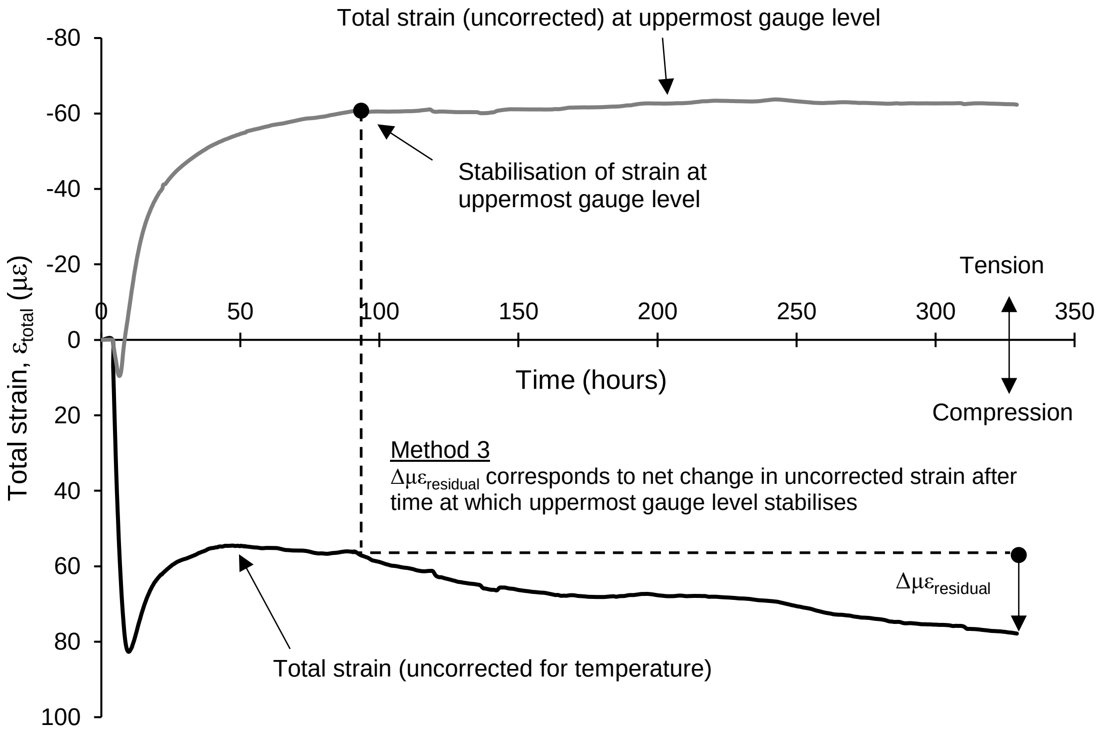

(b)

Figure 1. Interpretation of residual loads during curing using continuous strain measurements – (a) Method 2 and (b) Method 3

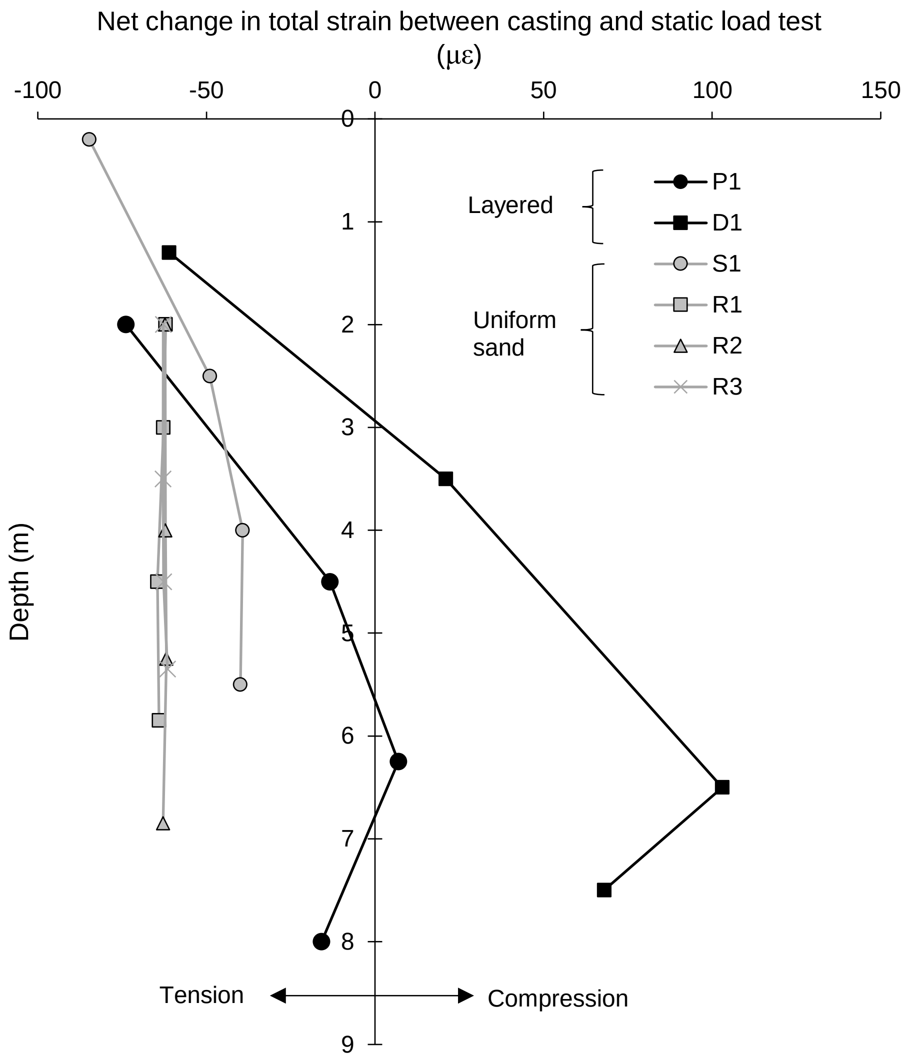

Figure 2. Net change in total strain between casting and commencing static load test for selected DCIS piles in Table 1

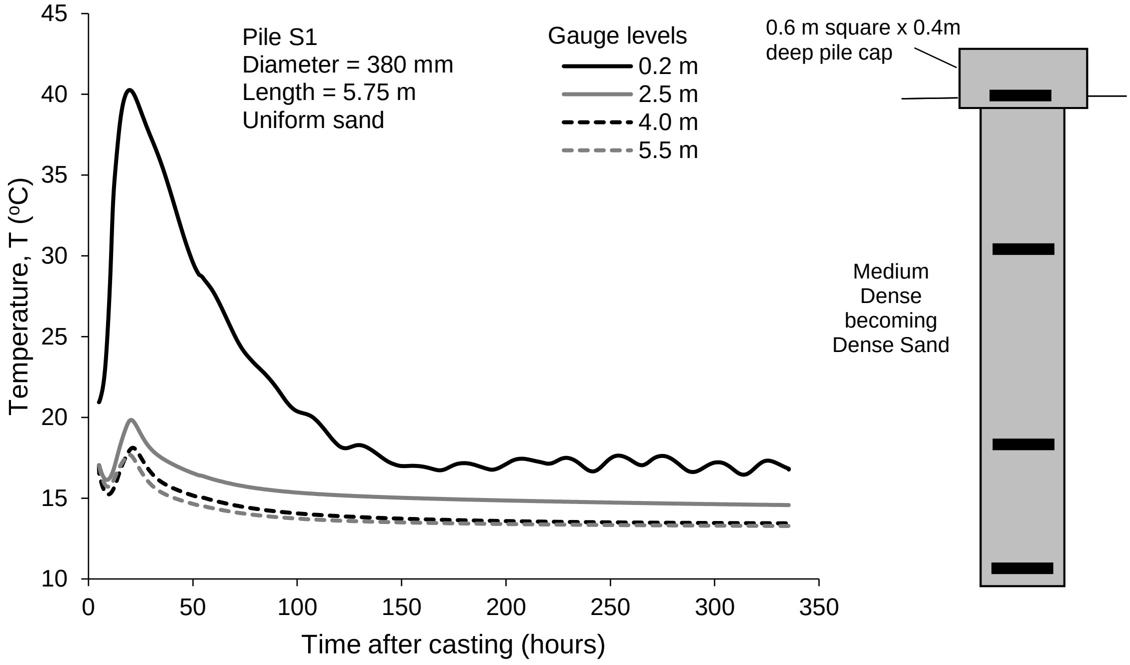

(a)

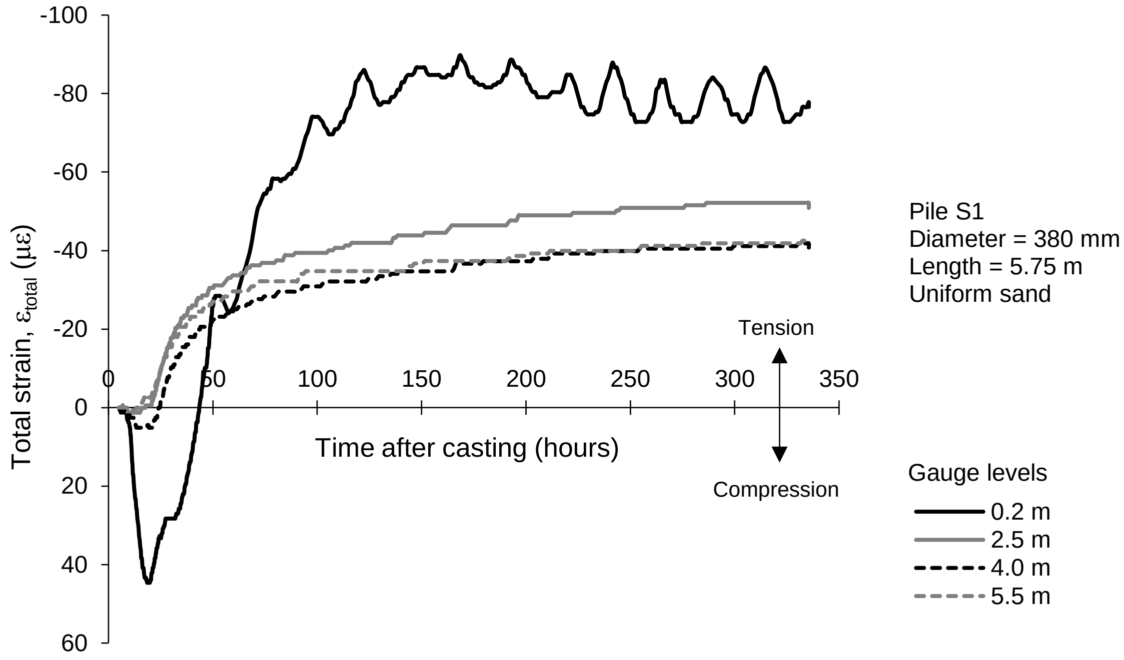

(b)

Figure 3. Variation with time after casting of (a) temperature and (b) strain – Pile S1 in uniform medium dense to dense sand

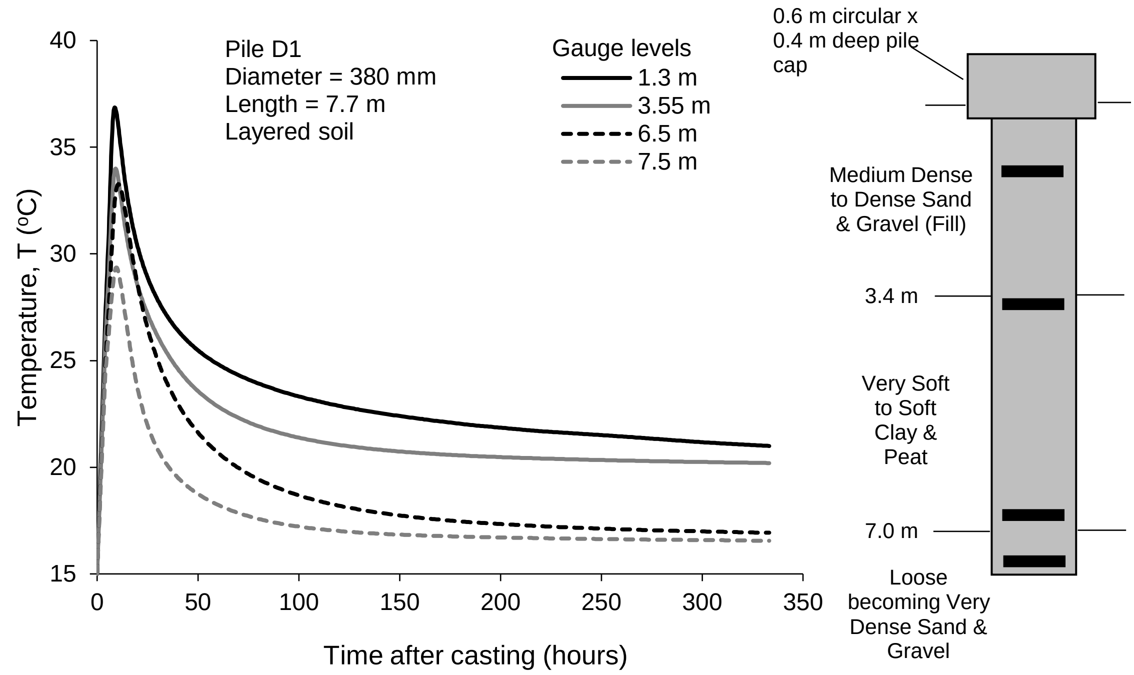

(a)

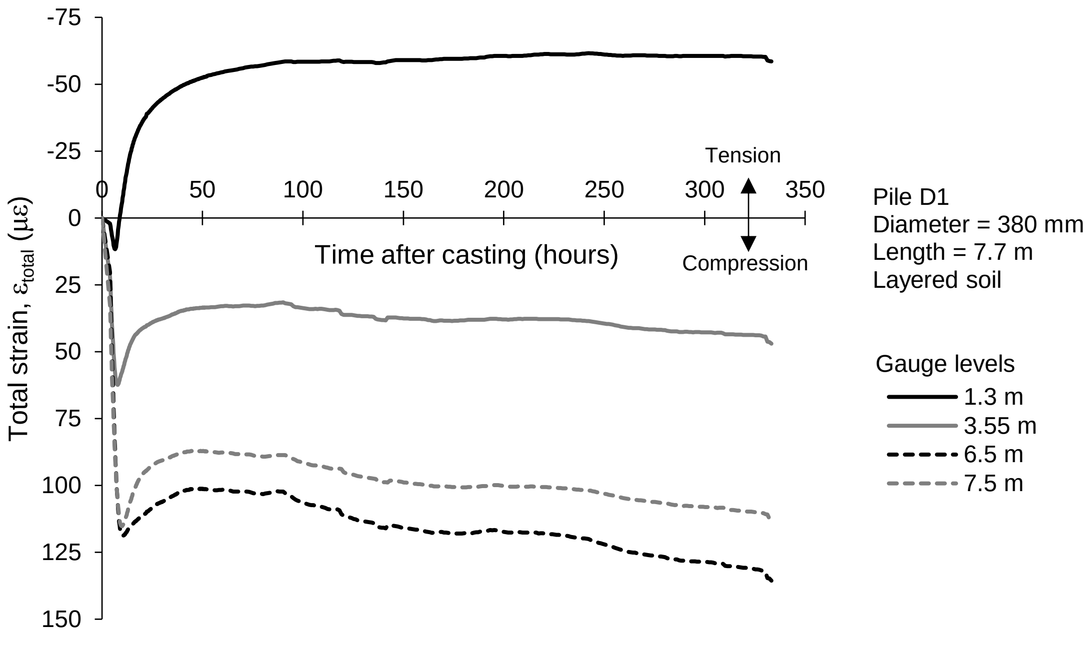

(b)

Figure 4. Variation with time after casting of (a) temperature and (b) strain – Pile D1 in layered soil

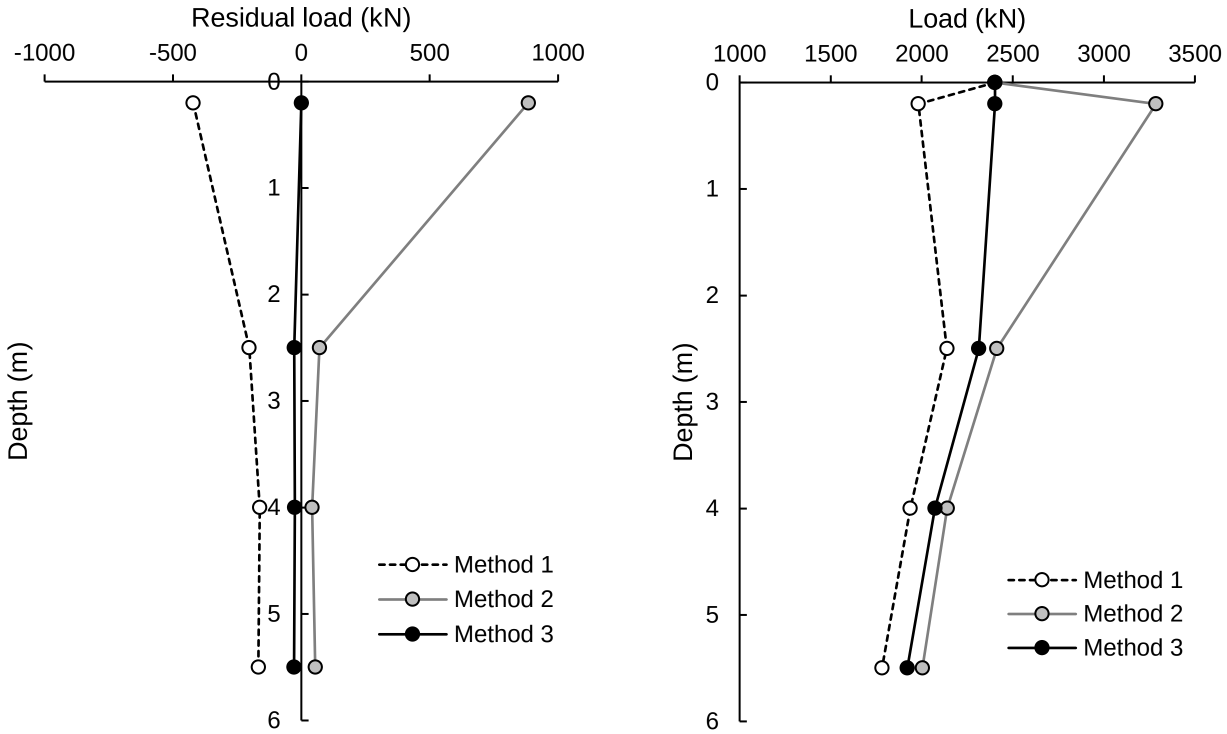

(a)

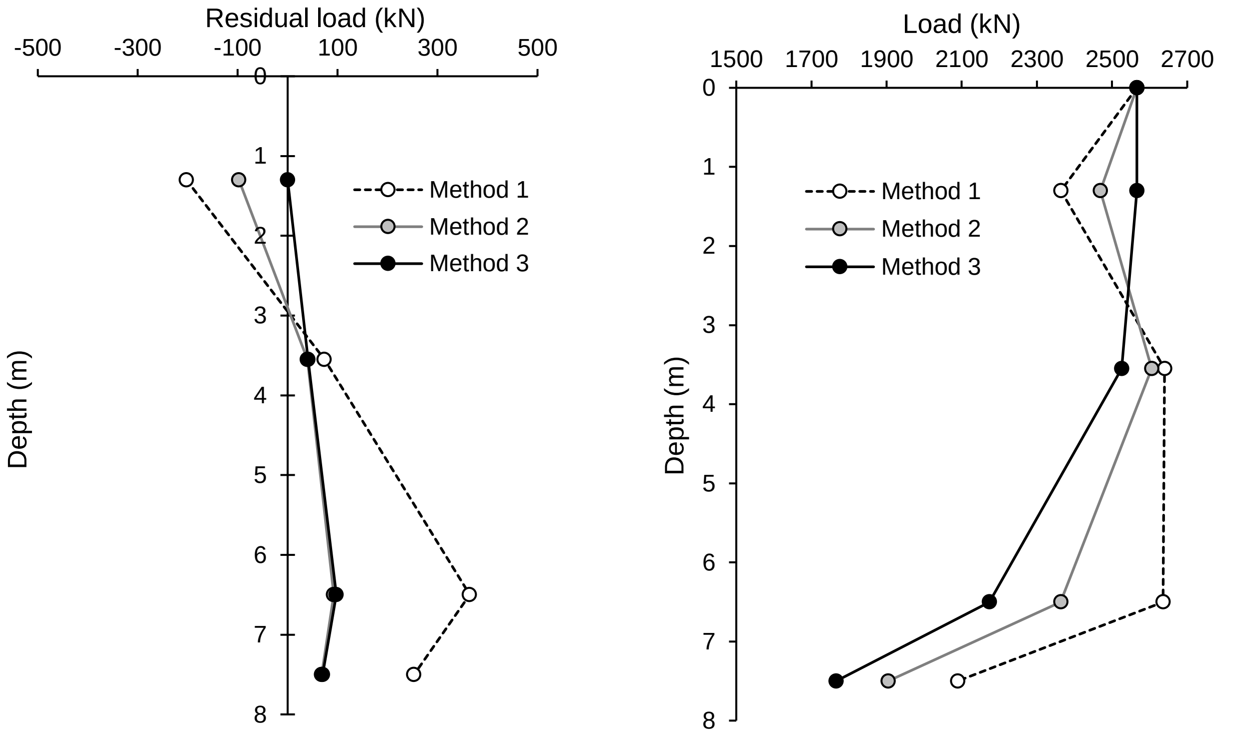

(b)

Figure 5. Interpreted residual load distribution during curing and ultimate load distribution during static load testing for (a) Pile S1 in uniform sand and (b) Pile D1 in layered soil

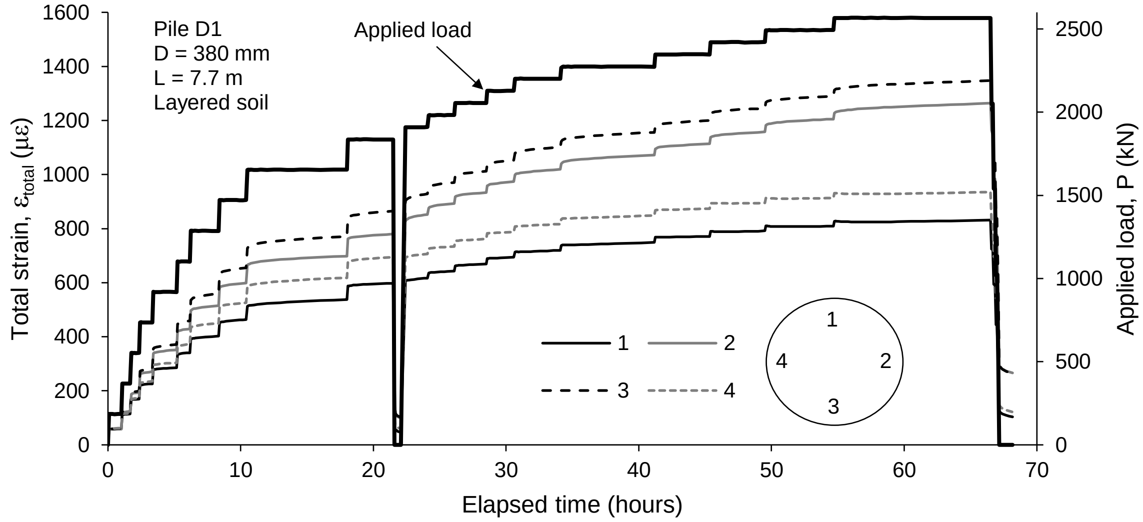

(a)

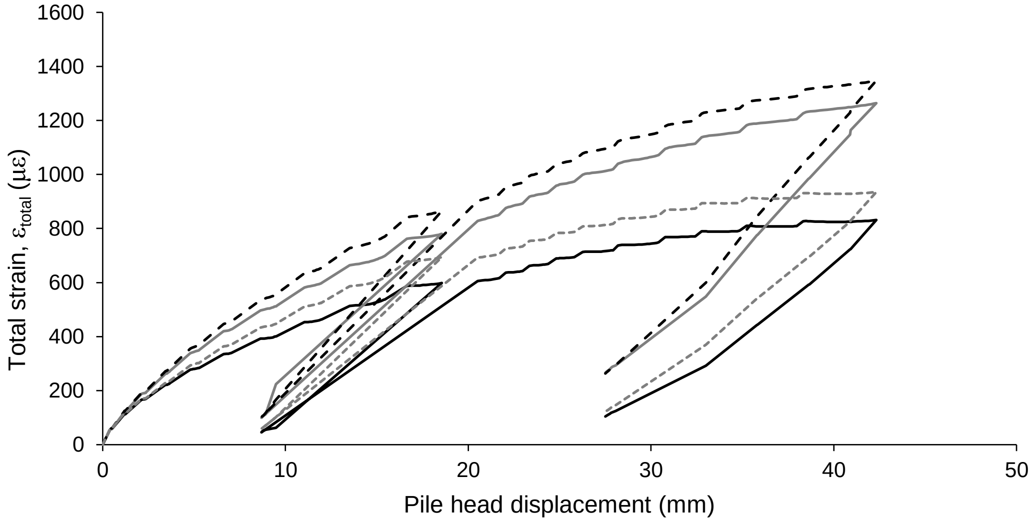

(b)

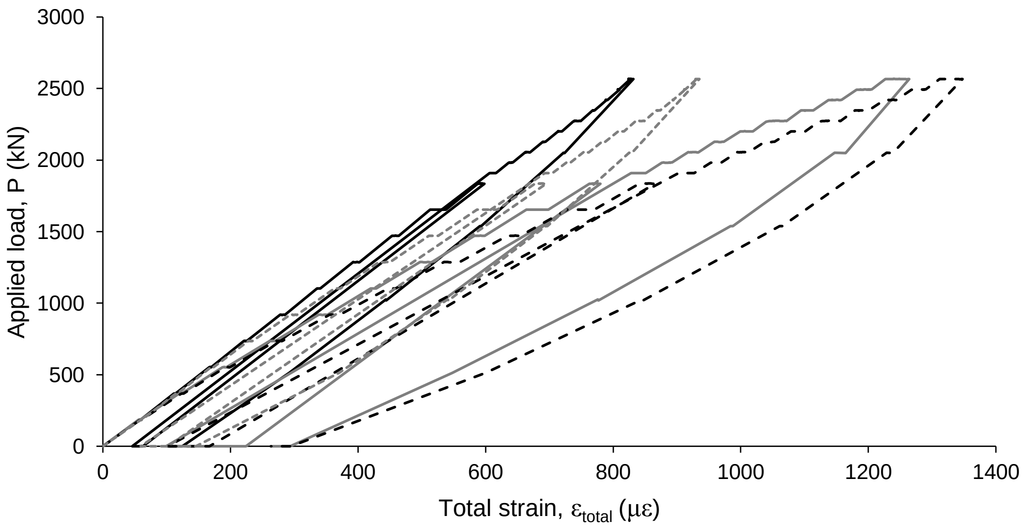

(c)

Figure 6. Variation of (a) strain and applied load with time, (b) strain with displacement and (c) strain with applied load during static compression load test at uppermost gauge level of Pile D1 in layered soil

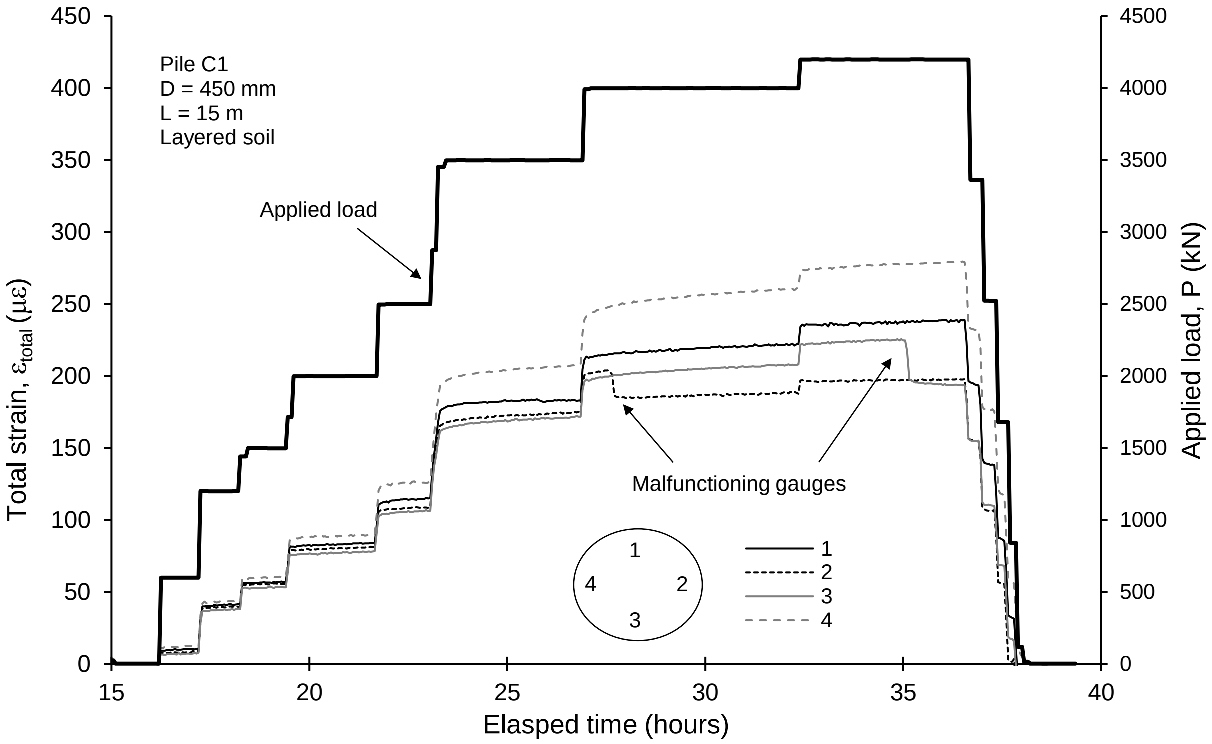

Figure 7. Example of malfunctioning strain gauges during static compression load test on Pile C1 in layered soil

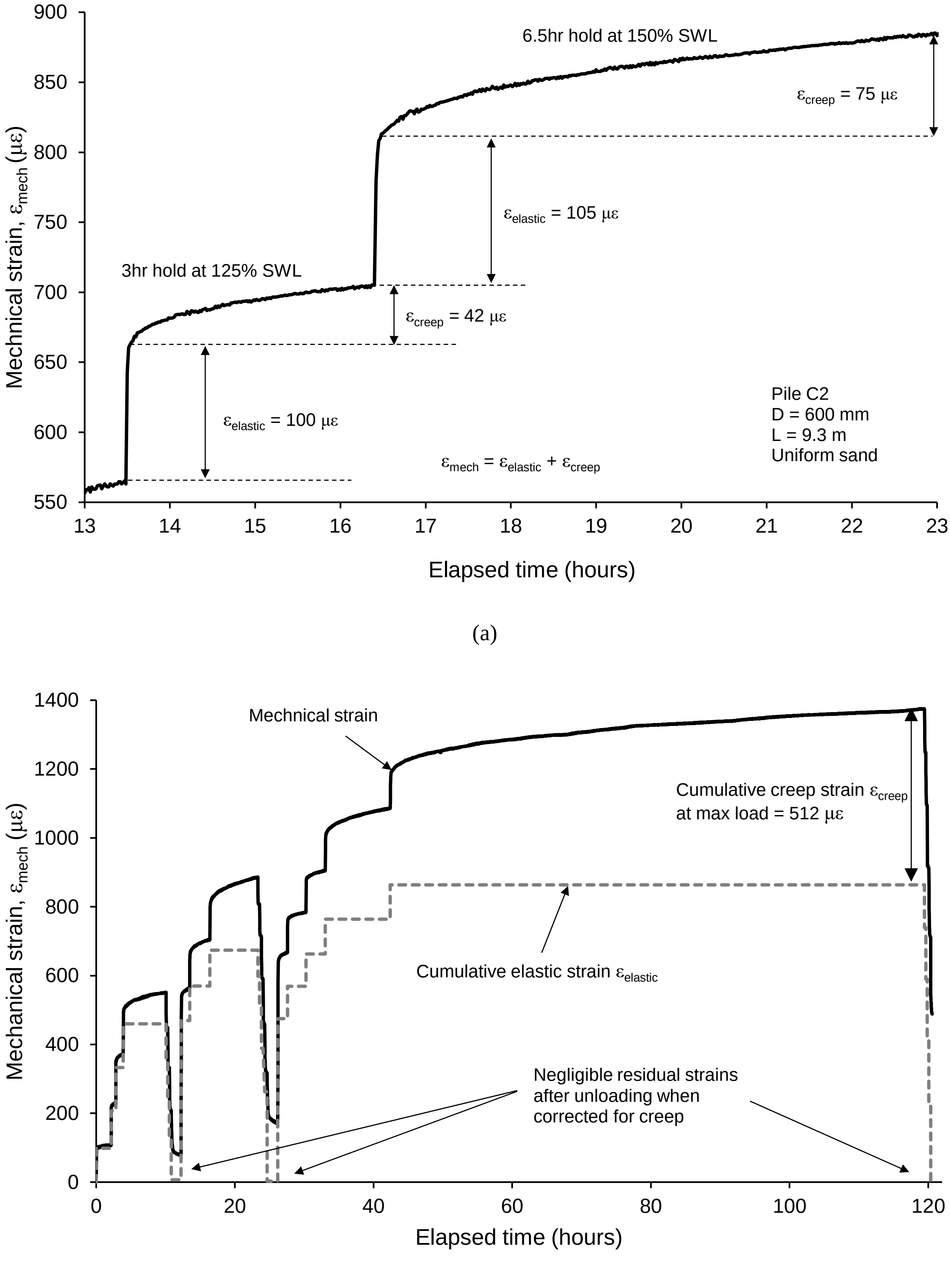

(a)

(b)

Figure 8. (a) Elastic and creep strains during maintained compression load test and (b) mechanical and creep-corrected strain response of Pile C2 in uniform sand

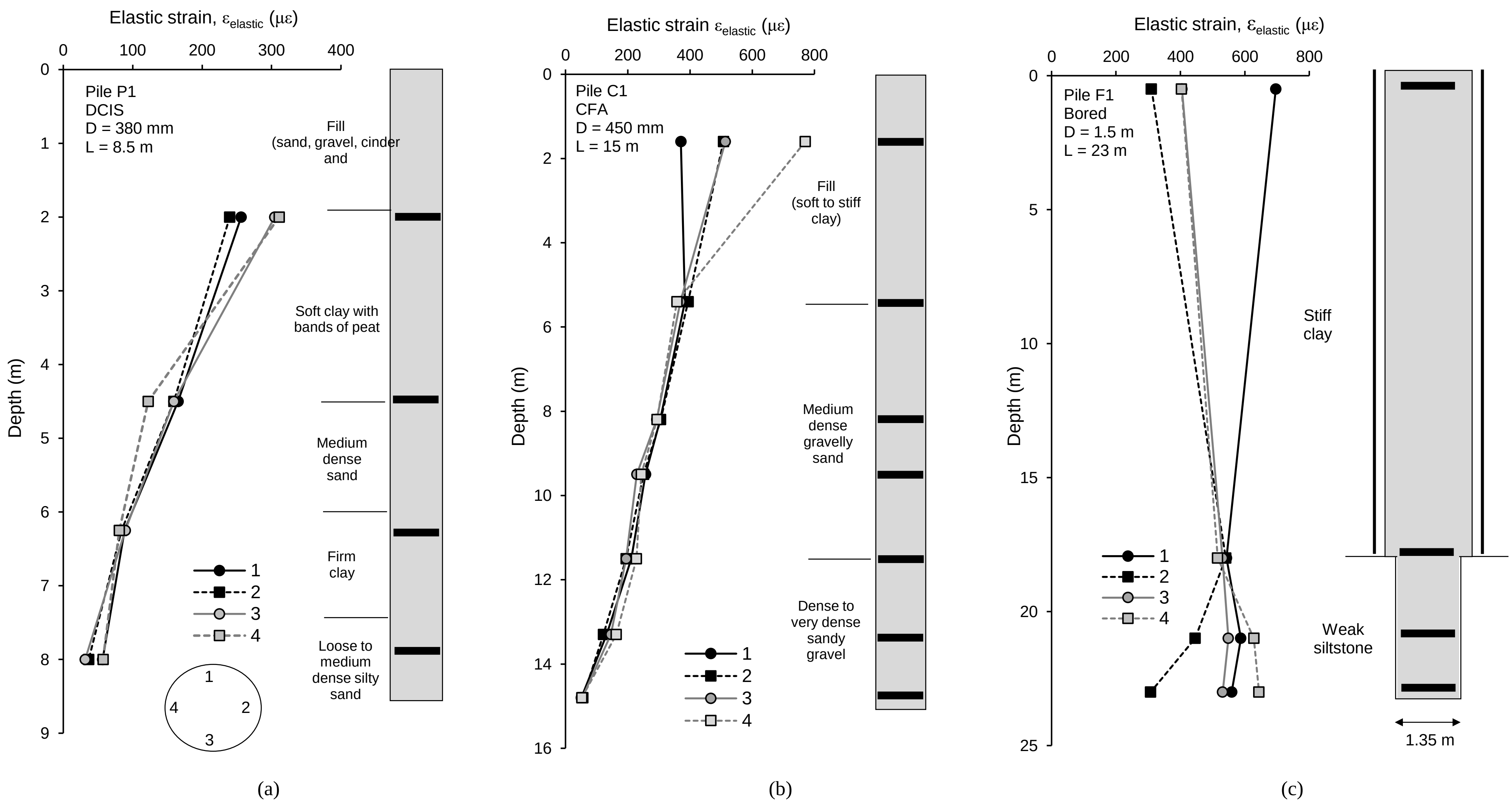

Figure 9. Examples of strain distribution with depth at maximum applied load for (a) Pile P1 in layered soil, (b) Pile C1 in layered soil and (c) Pile F1 in rock with double sleeved casings in overburden

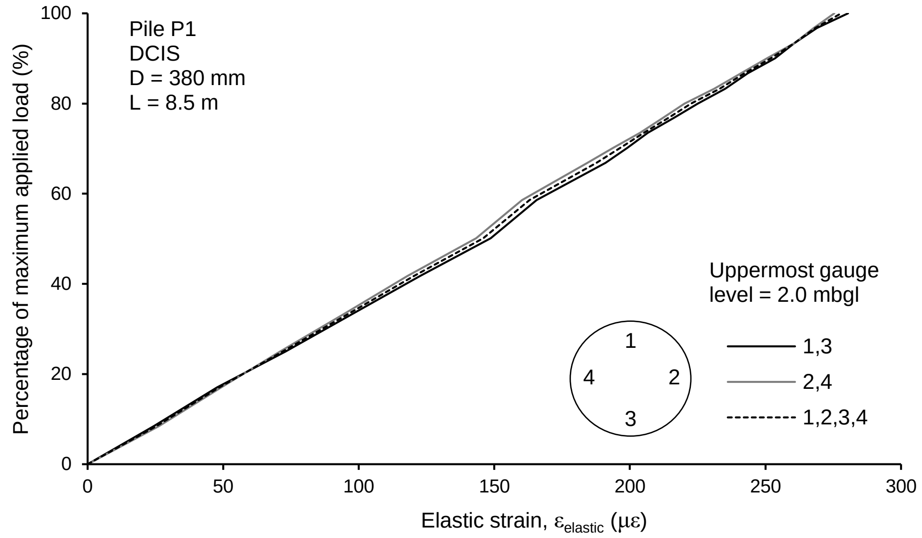

(a)

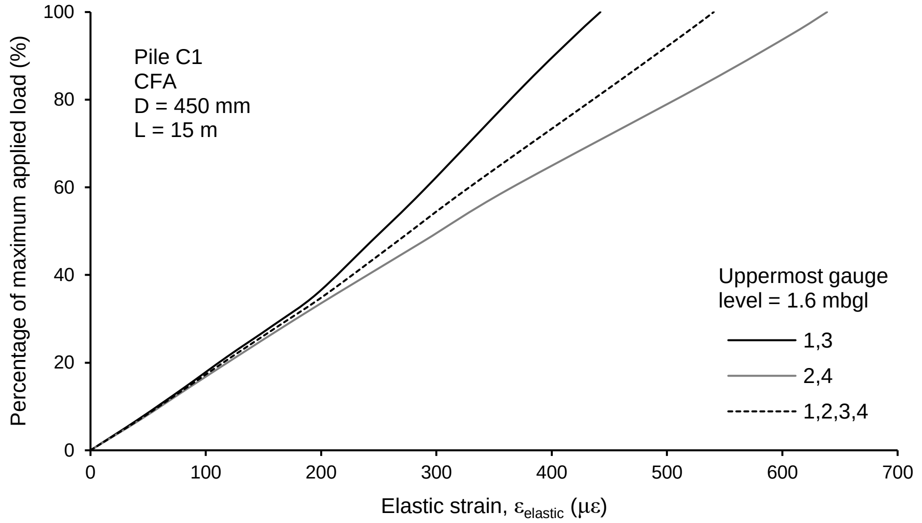

(b)

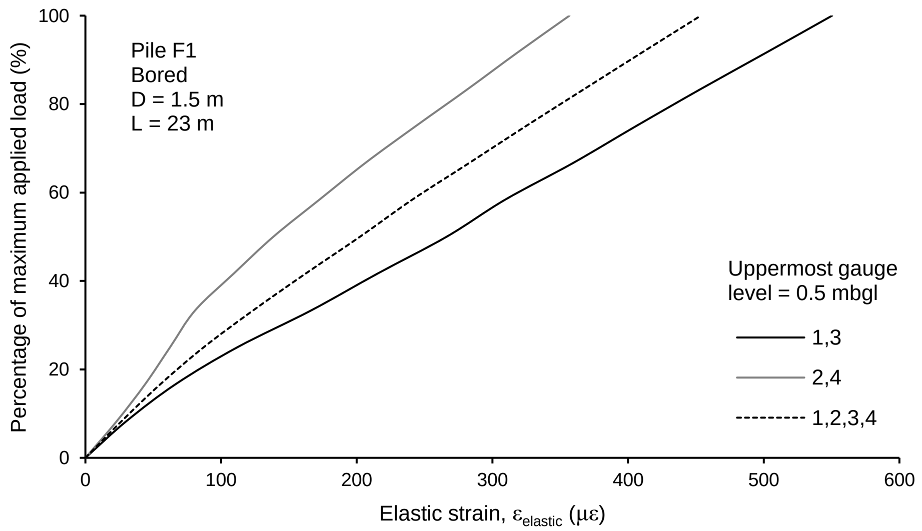

(c)

Figure 10. Effect of pile bending on average strains at uppermost gauge level during loading for (a) Pile P1 in layered soil, (b) Pile C1 in layered soil and (c) Pile F1 in rock with double sleeved casings in overburden

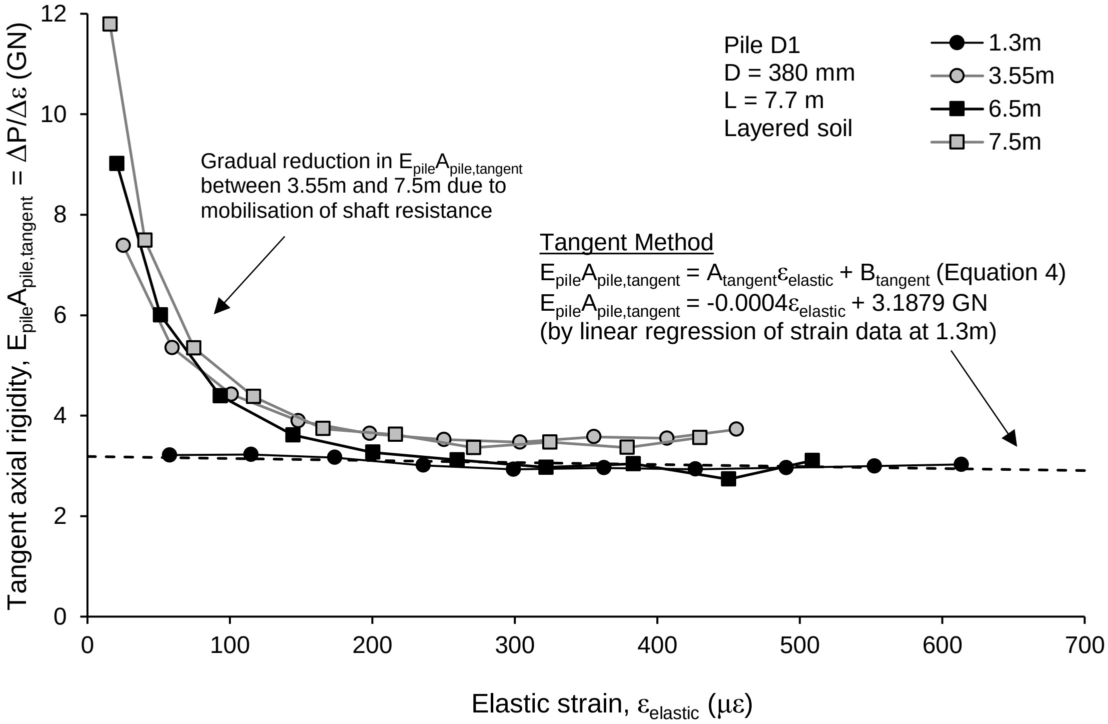

(a)

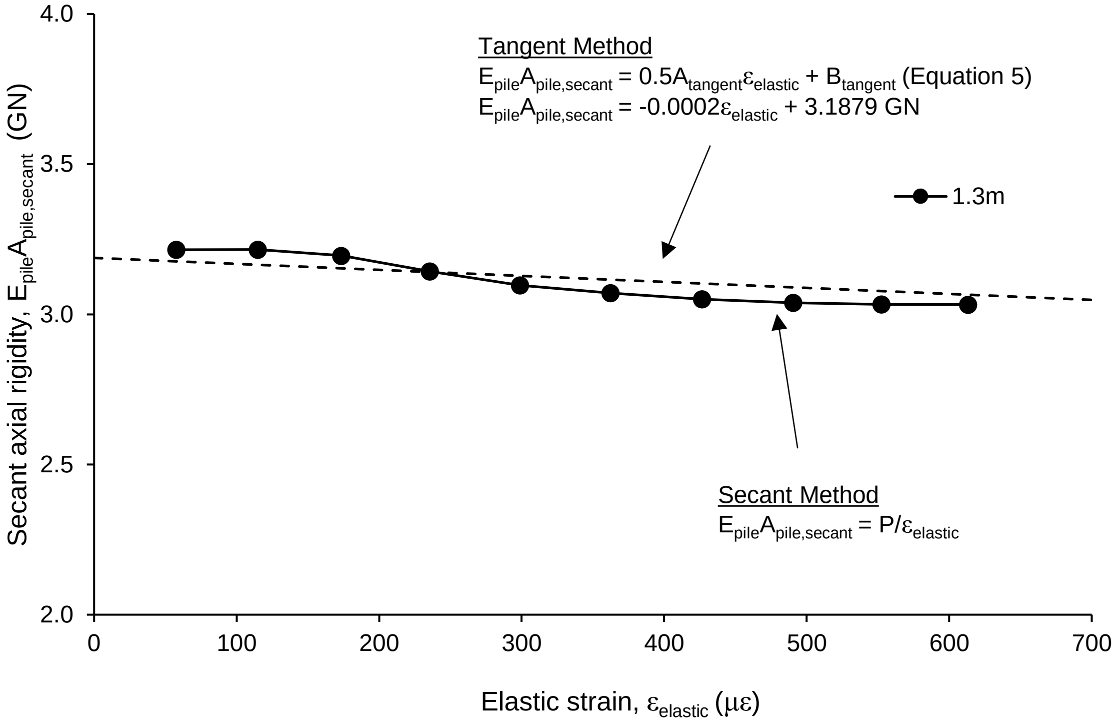

(b)

Figure 11. Variation with elastic strain of (a) tangent axial rigidity and (b) secant axial rigidity for Pile P1 in layered soil

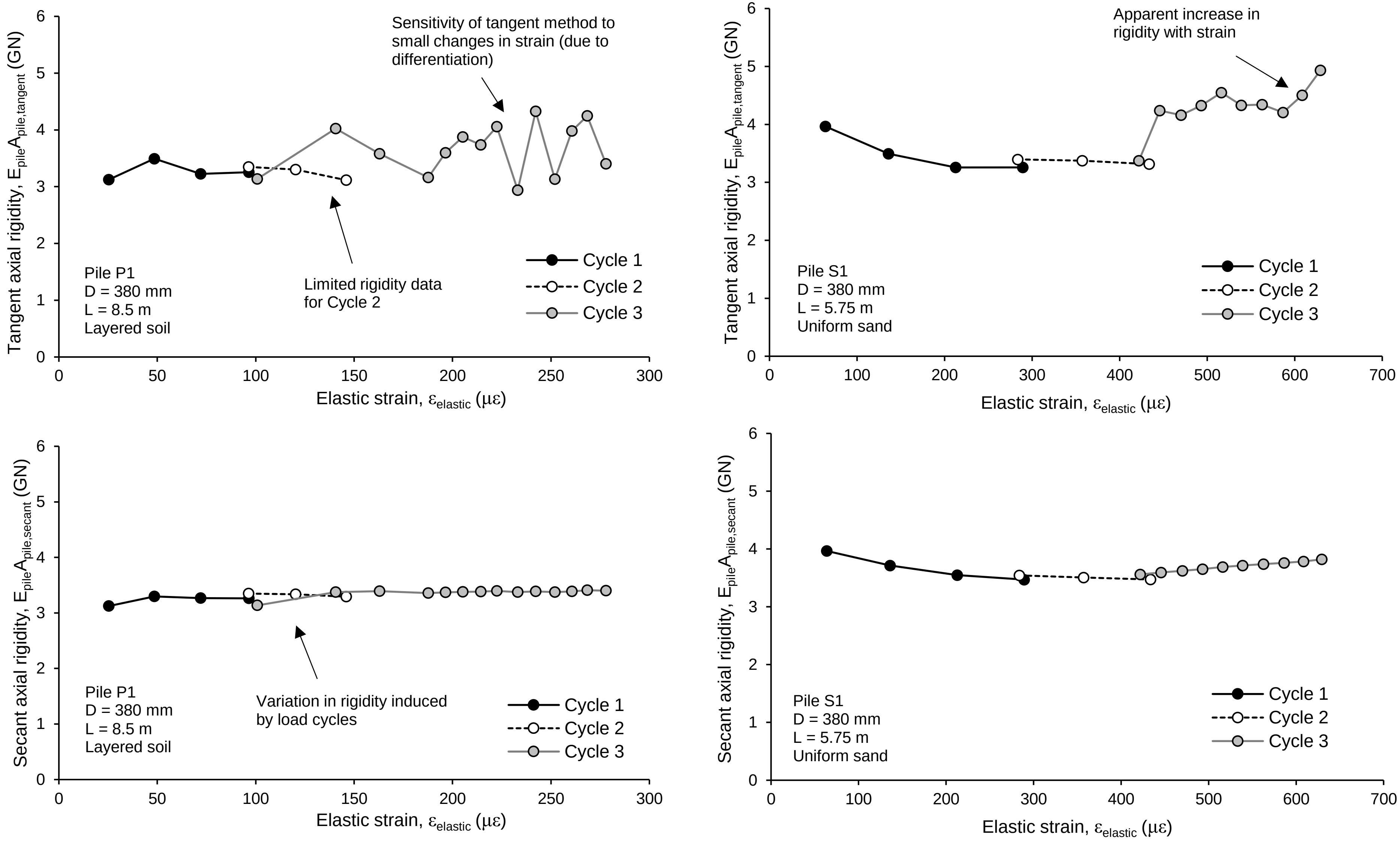

(a) (b)

Figure 12. Influence on tangent and secant axial rigidities of (a) multiple load cycles for Pile P1 in layered soil and (b) strain hardening during loading of Pile S1 in uniform sand

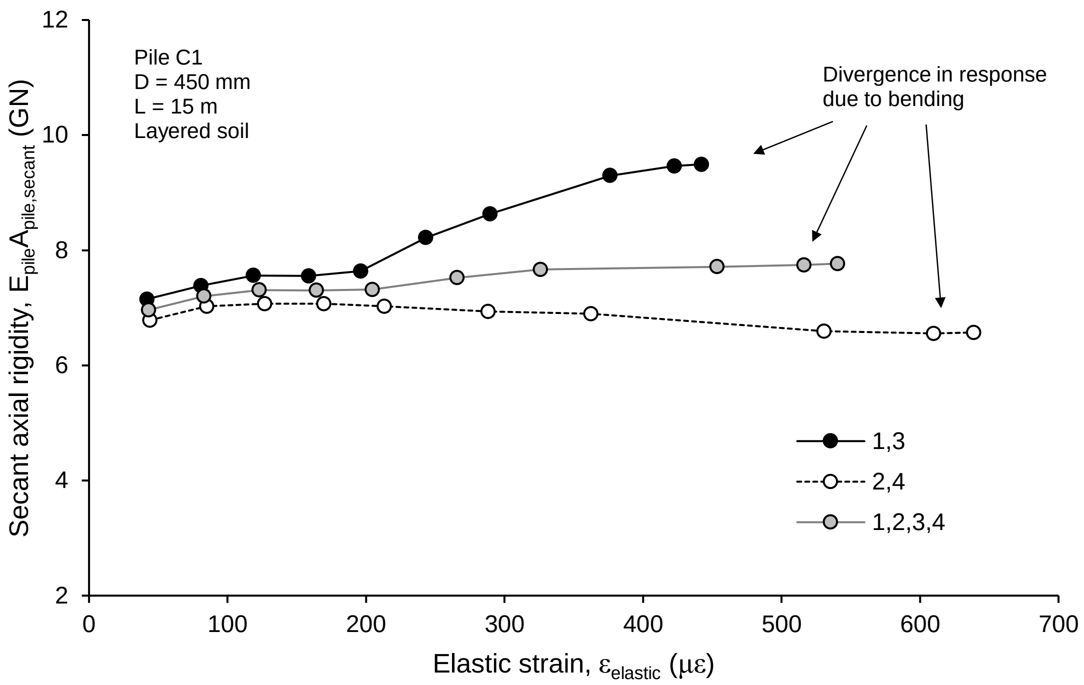

Figure 13. Effect of pile bending on secant pile axial rigidity of Pile C1 in layered soil

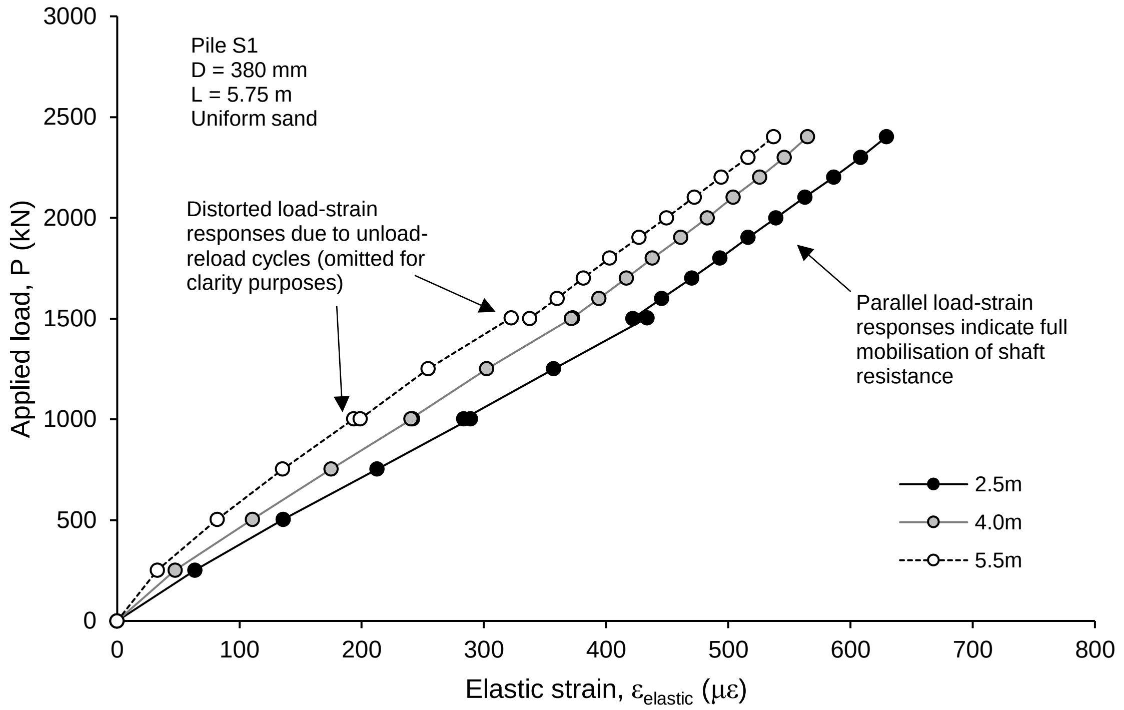

(a)

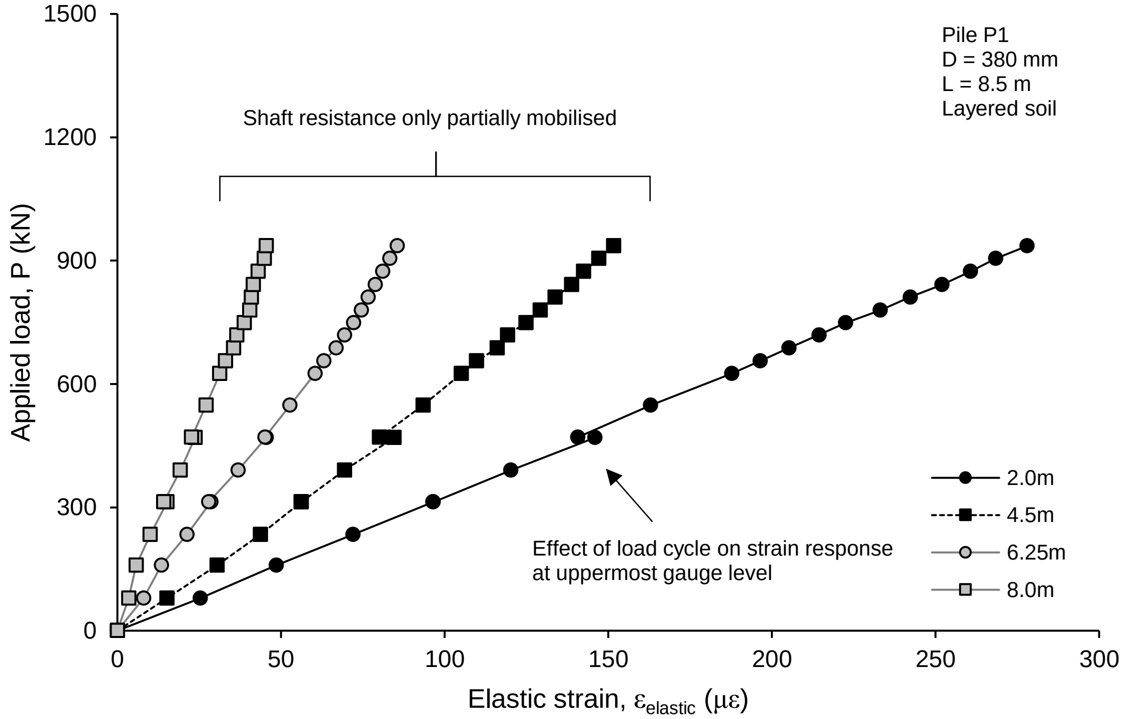

(b)

Figure 14. Variation in average elastic strain at each gauge level with applied load, highlighting (a) full mobilisation of shaft resistance for Pile S1 in uniform sand and (b) partial mobilisation of shaft resistance for Pile P1 in layered soil

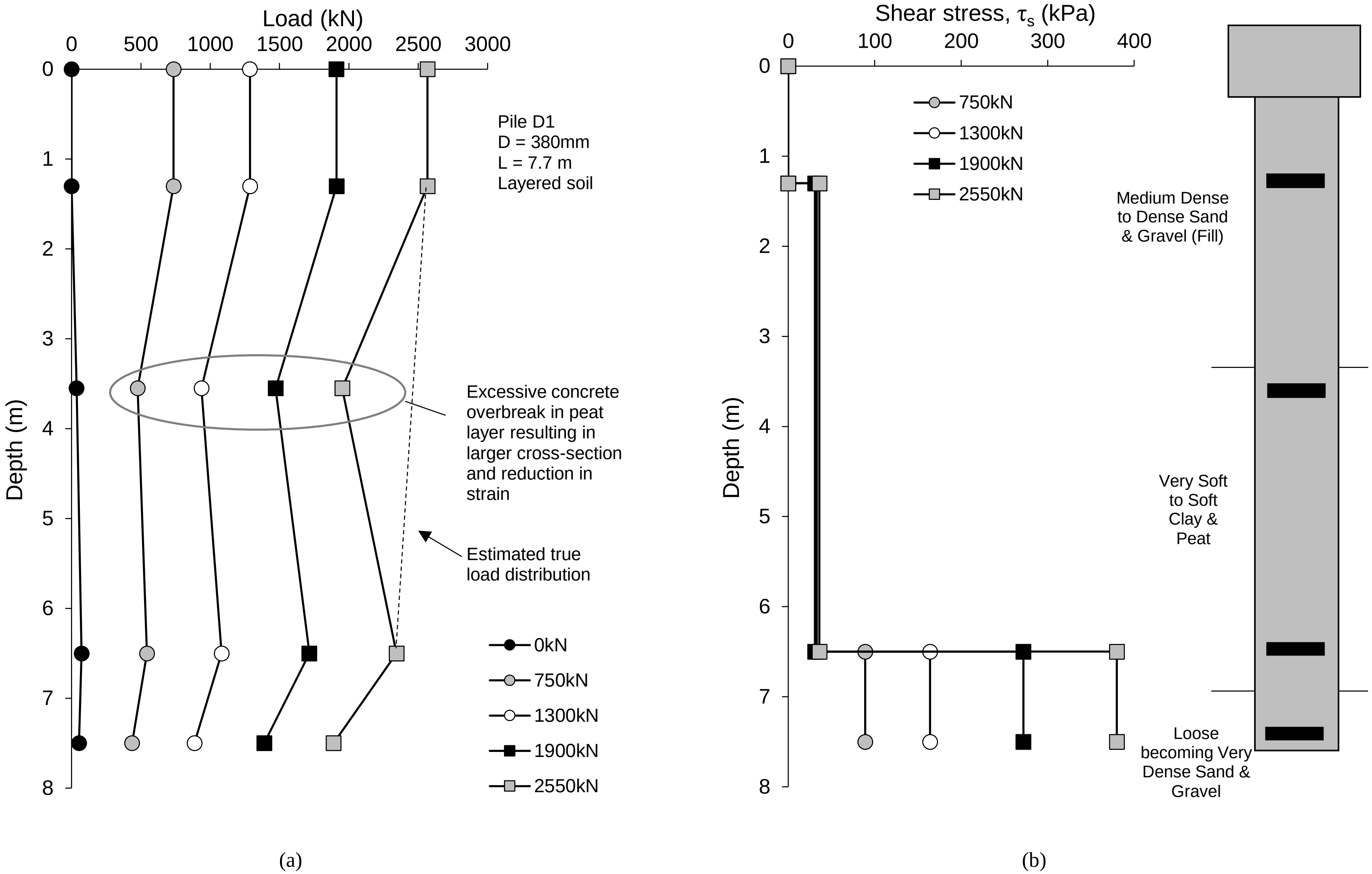

Figure 15. Variation with depth of (a) load and (b) shear stress for Pile D1 in layered soil

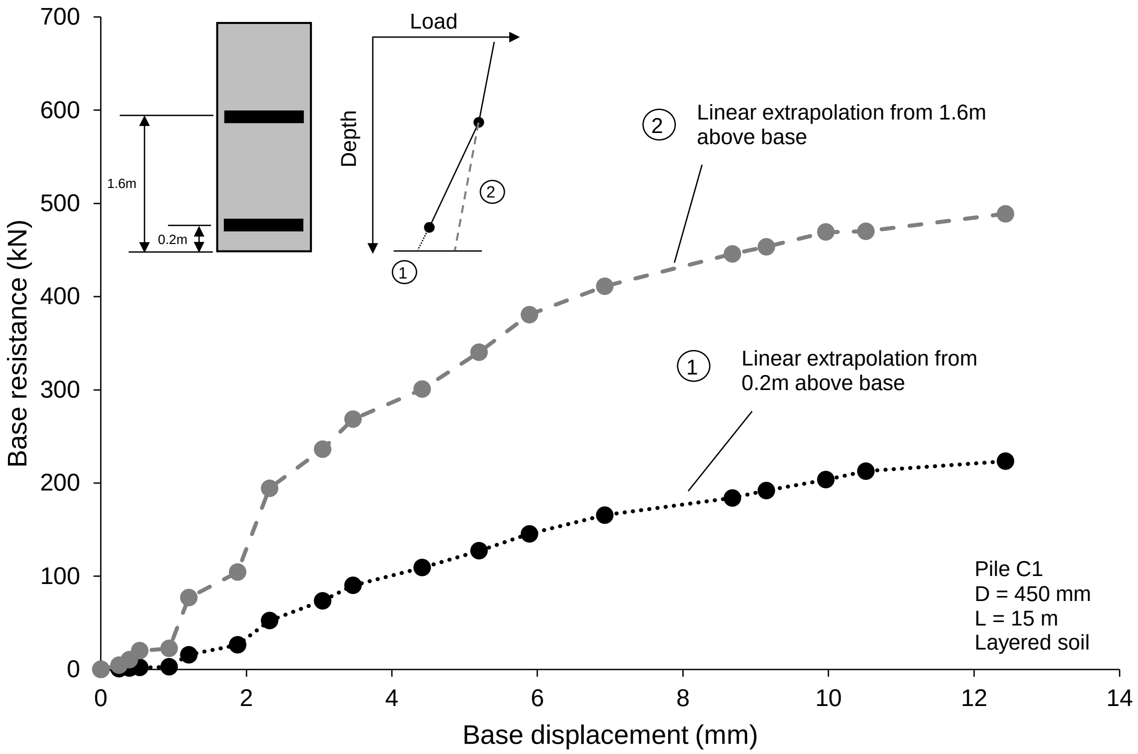

Figure 16. Effect of gauge distance from pile base on extrapolation for determining base resistance during maintained compression loading of Pile C1 in layered soil